nature communications

Article

https://doi.org/10.1038/s41467-025-67437-6

Manganese-engineered *Lactobacillus Reuteri* with enhanced antitumor and immunomodulatory activities for colorectal cancer prevention and treatment

Received: 20 March 2025

Accepted: 1 December 2025

Published online: 19 December 2025

Check for updates

Peng Cao[1,2,3,4,9], Qilin Li[1,2,3,4,9], Yuyu Li[1,2,3,4], Honglian Guo[1,2,3,4], Chunyu Wei[1,2,3,4], Rengui Xu[1,2,3,4], Chenke Ouyang[1,2,3,4], Wei Chen[5,6] ✉, Lin Wang[1,2,3,4,7] ✉ & Zheng Wang[2,3,4,7,8] ✉

Probiotic-based biotherapy for colorectal cancer (CRC) faces significant challenges due to poor tumor-targeting and limited bioactivities within the complex tumor microenvironment. This study shows that *Lactobacillus reuteri (L. reuteri)*'s inherent bioactivities, including proliferation, metabolism, and colorectal colonization, can be enhanced by manganese, prompting the fabrication of a manganese-engineered strain (MnLR). Oral administration of MnLR with its metabolic substrate-glycerol (MnLR/Gly) promotes the enrichment of *L. reuteri* and its antitumor metabolites within colon tumors. Across multiple preclinical colon tumor models, MnLR/Gly alone achieves a 95.6% inhibition of orthotopic tumor growth, liver metastases reduction by 62.1%, and confers durable protection, with 75% of prophylactically treated mice remaining long-term tumor-free and 62.5% resisting tumor rechallenge. Mechanistically, MnLR/Gly induces both intratumoral and peripheral dendritic cell maturation, M1 macrophage polarization, and effector T-cell responses. In orthotopic CRC rabbit models, GlyMnLR enteric capsules demonstrate significant antitumor efficacy comparable to standard chemotherapy while exhibiting favorable safety. These findings highlight MnLR as an effective standalone probiotic therapy for CRC prevention and treatment.

Colorectal cancer (CRC) ranks as the third most commonly diagnosed cancer and the second leading cause of cancer-related death worldwide, accounting for nearly 10% of the new cancer cases and deaths in 2020[1]. Effective interventions are still lacking, especially for distant metastatic CRC that decreased the 5-year survival rate to only ~10%[2]. The principal treatment option for both primary and metastatic CRC remains chemotherapy, which is, however, challenged by inevitable drug resistance and adverse reactions. Moreover, there are currently no well-established pharmacological strategies capable of preventing or delaying the occurrence of CRC. While non-steroidal anti-inflammatory drugs, such as aspirin and celecoxib, have shown potential preventive effects against CRC, their clinical feasibility remains uncertain[3,4]. Long-term use of these drugs can lead to gastrointestinal bleeding and elevate the risk of cardiovascular disease[4,5]. The significant development of immunotherapy has now revolutionized the field of oncology. However, in CRC, only a minority of metastatic patients with DNA mismatch repair-deficient (dMMR)/microsatellite instability-high (MSI-H) are potentially sensitive to immune checkpoint inhibitors. Most CRC patients are poorly responsive to immunotherapy due to low tumor neoantigen load, insufficient

A full list of affiliations appears at the end of the paper. ✉e-mail: weichen86@hust.edu.cn; lin_wang@hust.edu.cn; zhengwang@hust.edu.cn

immune cell enrichment, and the inherent presence of immunosuppressive components within the tumor microenvironment, such as macrophages with an immunosuppressive phenotype[6,7]. Thus, novel preventive and therapeutic strategies are highly desired for CRC.

A growing body of evidence reveals that the host microbiota within the gastrointestinal (GI) tract and other niches highly implicates the development of CRC[8], leading to new targets for medical intervention. Typically, the use of intestinal probiotics (*e.g., Lactobacillus* and *Bifidobacterium*) provides a safe and promising approach for CRC prevention and treatment due to their safety and potential to restore tumor-induced gut microbial dysbiosis, enhance the immune system, and directly inhibit tumor growth with their antitumor metabolic products[9,10]. However, current preclinical and clinical studies on probiotics in cancer prevention and treatment largely focus on their role as adjuvants to improve the efficacy and safety of chemotherapy and immunotherapy, rather than as standalone anticancer agents[11–14], most likely due to the uncertain efficacy, mechanism, and safety in the complex human body. Significant advancements in interdisciplinary research among microbiology, bioengineering, chemistry, and material science have brought various genetically, chemically, and physically engineered bacteria with augmented functionalities[15–17]. Despite these strides, the continued development and clinical translation of these bacteria formulations for cancer therapy still face substantial impediments mainly arising from the complicated and low-yield preparation process, ethical concerns, and notably, the limited antitumor effects owing to the lack of tumor-targeting capability and the progressive decline in bacterial activity and quantity before reaching target sites, concomitantly with inadequate production of antitumor metabolites[18–20]. Therefore, realizing the full potential of probiotics in CRC management requires identifying and developing bacterial strains with enhanced antitumor efficacy through in-depth investigations of their biological functions and optimizing their dosage formulations to ensure the effective and safe usage of probiotics in the host.

Lactobacillus reuteri (*L. reuteri*) is a well-defined probiotic bacterium that naturally inhabits the GI tract of humans and many other animals[20]. *L. reuteri* is known to produce various bioactive metabolites, including organic acids, antimicrobial compounds, and nutrients, which can inhibit the growth of pathogenic bacteria, protect against infections, and contribute to overall health[21–23]. *L. reuteri* has shown promise in the fight against several common pathological conditions, such as infant colic, constipation, diarrhea, *Helicobacter pylori* infection, colitis, and autoimmune disorders[24–26]. Recent studies suggest that *L. reuteri* is significantly reduced in CRC-bearing mice and patients' feces and tumor mucosa. Moreover, *L. reuteri*-derived metabolic products (*e.g.*, reuterin and indole-3-aldehyde) presented efficacy in suppressing CRC growth by altering redox balance and improving immune checkpoint inhibitor response in melanoma[27,28]. Nevertheless, the multifaceted impacts of *L. reuteri* on complex cancer biological processes and its potential roles in cancer prevention and treatment remain poorly understood.

Metal ions (*e.g.*, iron, copper, zinc, and manganese) are essential for supporting the survival, growth, and biochemical reactions of bacteria at a suitable level by maintaining bacterial structural stability, enhancing their catalytic activity, and regulating gene expression or signal transduction[29–32]. For instance, manganese (Mn) supports bacterial oxidative stress resistance through Mn-dependent antioxidant systems[33,34], and modulates host innate immune signaling pathways to enhance antiviral and antitumor effects[35,36]. These properties make Mn modification especially suitable for customizing bacterial biological properties to withstand challenging environments and enhance functionality.

Here, we reveal that Mn enhances the proliferation, metabolic activity, and colorectal colonization of *L. reuteri*, enabling the development of a Mn-modified strain (MnLR) with improved bioactivity. MnLR combined with glycerol shows increased intratumoral accumulation and metabolite production, resulting in strong suppression of orthotopic colon tumors through cancer-selective cytotoxicity, restoration of tumor-induced dysbiosis, and activation of antitumor immunity. To facilitate translational application, we further formulate an enteric GlyMnLR capsule that achieves robust efficacy and favorable safety in a rabbit CRC model. Together, this study establishes MnLR as a highly efficient, safe, and cost-effective oral microbial agent with broad implications for CRC prevention, treatment, and future development of engineered probiotic therapeutics.

Results

L. reuteri-derived glycerol metabolites exhibit redox-dependent CRC inhibition and enrich multiple tumor-associated immune cells within colon tumors

The CRC-inhibitory effects of the metabolites produced by *L. reuteri* catabolizing glycerol were determined in vitro (colon cancer cell lines and organoids from CRC patients) and in vivo (subcutaneous colon cancer-bearing mice) (Fig. 1a). Reuterin (*i.e.*, 3-hydroxypropionaldehyde (3-HPA)) is a bioactive intermediate in glycerol catabolism and has been determined to be capable of inhibiting CRC growth by altering redox balance in cancer cells[27]. Consistent with the previous findings[27], the mixed metabolites from *L. reuteri* catabolizing glycerol exerted a potent growth-inhibitory effect preferentially on cancer cells over non-cancerous cells in a redox-dependent manner (Fig. 1b, c), as the metabolites stimulated the production of cytotoxic reactive oxygen species (ROS), reduced antioxidative glutathione level, and upregulated oxidative stress–related molecules at both the mRNA and protein levels in colon cancer cells (Supplementary Fig. 1); and their cytotoxic effect was significantly reduced in human normal colonic epithelial cells (NCM460), human umbilical vein endothelial cells (HUVEC), and normal human liver cells (L-02) (with the cell viability remaining above 80% at a reuterin concentration of 50 μg/mL), as well as in the presence of *N*-acetyl-cysteine (NAC, a ROS scavenger) (Fig. 1b, d). Notably, mass spectrometry analysis revealed the presence of various compounds from glycerol catabolism within the mixed metabolites in addition to reuterin, including reuterin's downstream products and nearly 20 unidentified compounds (at a percentage of > 0.1%) (Supplementary Table 1). Furthermore, the growth-inhibitory efficacies of the pure reuterin and its downstream products (1,3-propanediol and 3-hydroxypropionic acid) on colon cancer cells were lower in comparison to the mixed metabolites (containing an equivalent amount of reuterin) (Fig. 1b and Supplementary Fig. 2), indicating the potential cytotoxic effects of those unidentified metabolites on cancer cells. Consistent with these findings, reuterin elevated intracellular ROS levels in colon cancer cells, but to a markedly lower extent than the mixed metabolites (Supplementary Fig. 3); whereas its downstream products only caused a slight increase in ROS (Supplementary Fig. 3), suggesting that these products may exert cytotoxicity through ROS-independent or partially ROS-independent mechanisms. Further, the more effective colon cancer suppression of the mixed metabolites than pure reuterin was confirmed in five independent CRC patient-derived organoid (PDO) models, including four microsatellite stable (MSS) and one MSI-H subtypes (Fig. 1e, f, Supplementary Fig. 4, and Supplementary Table 2), supporting the robustness and clinical relevance[37].

Next, the in vivo antitumor efficacy of glycerol metabolites was examined using subcutaneous colon cancer-bearing mice that were treated with pure reuterin or glycerol metabolites either by intratumoral injection (i.t.) or oral gavage (o.g.). Consistent with the observations in vitro, the orally-delivered metabolites effectively suppressed tumor growth, with a tumor weight suppression rate of nearly 1.8-fold higher than oral reuterin, and 1.2-fold higher than intratumorally-injected metabolites (Fig. 1g and Supplementary Fig. 5). This finding suggests that the orally-delivered metabolites can be effectively distributed into tumors, and may even induce systemic impacts to promote antitumor effects. Thus, we analyzed the tumor-associated

https://doi.org/10.1038/s41467-025-67437-6

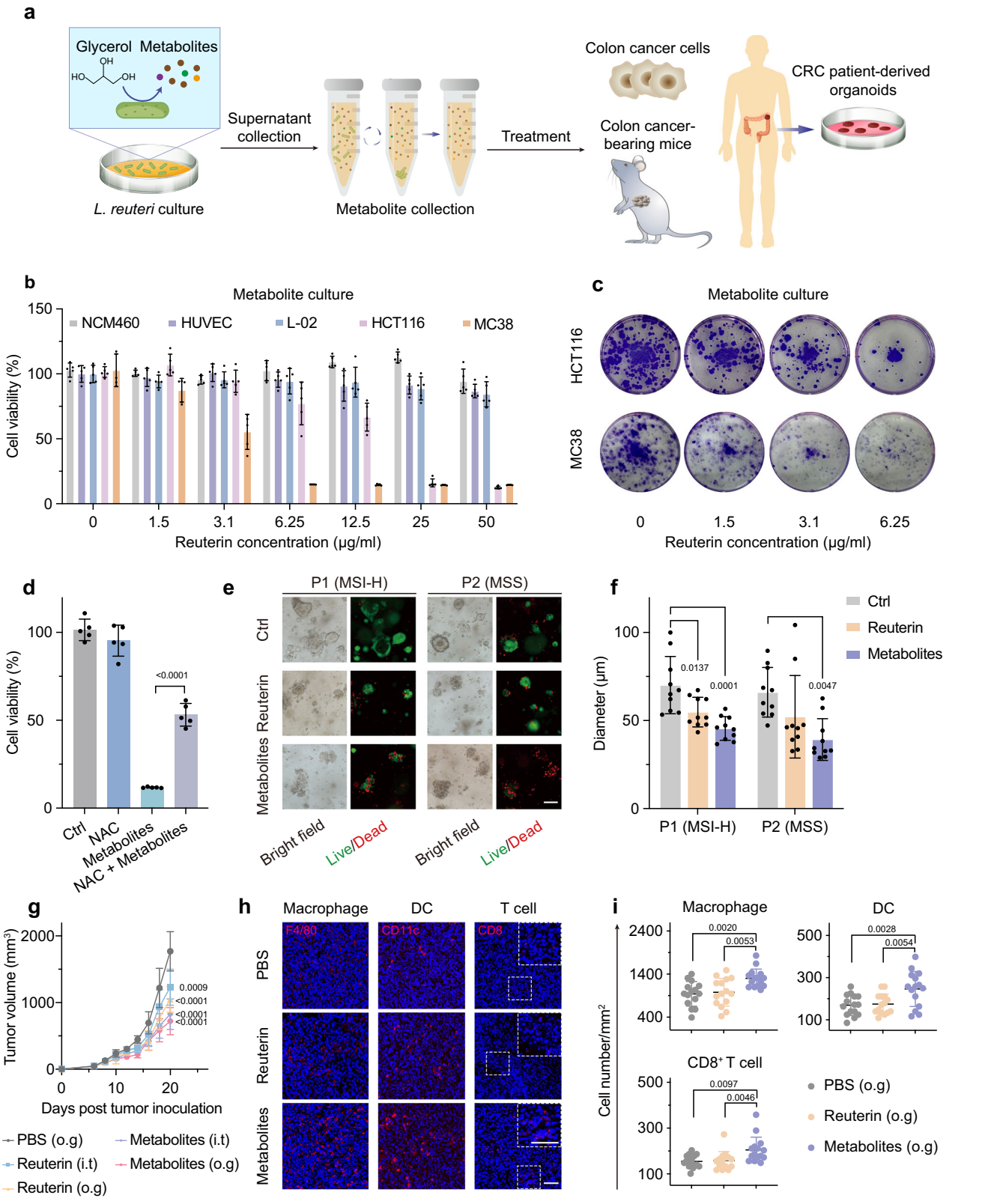

immune cells within the tumor tissues since the immune system plays a significant and complex role in CRC development and treatment[38–40]. Notably, the numbers of macrophages, DCs, and $CD8^+$ T cells were increased in the tumor microenvironment of the metabolite-orally treated mice (Fig. 1h, i), indicating that apart from the direct cytotoxicity in tumor cells, the metabolites might exert immunological impacts, potentially suppressing tumor growth.

L. reuteri is chemically modified with Mn that facilitates the proliferation, glycerol metabolism, and bio-adhesion of *L. reuteri*

Based on the aforementioned antitumor effects of *L. reuteri*-derived glycerol metabolites, we proposed modifying *L. reuteri* to enhance its proliferation and glycerol metabolism activities, aiming to achieve a high local concentration of antitumor metabolites for effective tumor

Fig. 1 | Glycerol metabolites from *L. reuteri* inhibit CRC growth in vitro and in vivo, and increase immune cells in colon tumors. a Schematic illustration of the culture of *L. reuteri* in glycerol, the centrifugal collection of glycerol metabolites, and the antitumor activity assessment in different cancer models. **b** Cell viabilities of NCM460, HUVEC, L-02, HCT116, and MC38 cells after a 24-hour culture with the collected metabolites at different reuterin concentrations (n = 5). **c** Colony-forming assay of HCT116 and MC38 cells treated with the metabolites at different reuterin concentrations. **d** Viabilities of MC38 cells after treatment with mixed metabolites (containing 6.25 μg/ml of reuterin) or pretreatment with 1.5 mg/ml NAC for 24 h (n = 5). **e** The representative microscopic and live/dead staining images of the PDOs derived from MSI-H and MSS CRC patients treated with pure reuterin (1.5 μg/ml) or mixed metabolites (containing 1.5 μg/ml of reuterin) for 3 days. Scale bar, 50 μm. **f** The organoid diameter after a 3-day treatment with the given agents (n = 10). **g** Tumor growth curves of subcutaneous MC38 cancer-bearing mice received an intratumoral injection (i.t.) or oral gavage (o.g.) of the given agents (n = 7). **h**, **i** The representative immunofluorescence staining images and the corresponding quantification of macrophages ($F4/80^+$), DCs ($CD11c^+$), and $CD8^+$ T cells within the tumor tissues from the mice receiving the given treatments (n = 15 fields from 3 mice per group). Scale bar, 50 μm. The area within the white box is shown magnified. The "n" represents the number of biologically independent samples. Data are shown as mean ± SD; p-value (compared to Ctrl in **f**; compared to PBS group in **g**); one-way ANOVA (one-tailed), Tukey's multiple comparisons test. Source data are provided as a Source Data file.

suppression. To this end, we incubated *L. reuteri* with diverse metal ions naturally present in the human body to identify specific metals capable of enhancing *L. reuteri*'s bioactivities. We found that the proliferation and glycerol metabolism (measured by the reuterin yield) of *L. reuteri* were simultaneously promoted by Mn in a concentration-dependent manner (Fig. 2a–d). Consistently, Mn enhanced the enzymatic activity of glycerol dehydratase (GDHt) that catalyzes the dehydration of glycerol into reuterin in *L. reuteri* (Supplementary Fig. 6a)[41]. The reduced *L. reuteri* proliferation and reuterin production in the presence of Mn ion chelating agents or oxidative phosphorylation uncouplers (for the inhibition of Mn ion uptake) further demonstrated the essential role of Mn in fostering *L. reuteri* (Supplementary Fig. 6b). Also, Mn^{2+} supplementation significantly promoted the proliferative and metabolic activities of *L. reuteri* under carbon or nitrogen deprivation (Supplementary Fig. 7), highlighting the specific biological role of Mn in sustaining and rescuing bacterial functionality under nutrient-limited conditions. Furthermore, to assess the long-term retention of Mn-mediated enhancements, *L. reuteri* strains were propagated up to the 50^{th} generation, with no significant differences observed in growth or glycerol metabolism compared with early passages (3^{rd} generation) (Fig. 2e), demonstrating generational stability. In addition, Mn^{2+} supplementation sustained enhanced bacterial proliferation and glycerol metabolism in simulated intestinal fluid (SIF) (Fig. 2f), indicating that these effects are durable under conditions relevant to CRC therapy. To investigate the underlying biological mechanisms by which Mn promotes *L. reuteri*'s bioactivity, prokaryotic transcriptomics were employed. Mn-treated *L. reuteri* was grouped in a cluster (Fig. 2g) and exhibited 130 up-regulated genes and 143 down-regulated genes compared with untreated *L. reuteri* (Supplementary Fig. 8). Furthermore, the subsequent pathway enrichment analysis determined that Mn-treated *L. reuteri* exhibited significant upregulation of signaling pathways related to the ribosome, thiamine metabolism, and oxidative phosphorylation, with ribosome pathways being the most prominent (Fig. 2h). To functionally validate these transcriptomic findings, quantitative proteomic analysis confirmed elevated levels of ribosomal proteins (Fig. 2i). SDS-PAGE further demonstrated increased global protein synthesis in Mn-treated *L. reuteri* (Supplementary Fig. 9). These results collectively establish that the transcriptional upregulation of ribosome-related pathways is functionally translated into enhanced ribosomal activity and protein synthesis, suggesting that ribosomes may be a key target for the regulation of *L. reuteri*'s bioactivity by Mn ions[42].

Subsequently, we set out to modify *L. reuteri* with Mn using tannic acid (TA) as a chemical linker to obtain a bioactivity-enhanced *L. reuteri* (MnLR) (Fig. 2j). The successful surface modification of Mn on *L. reuteri* was verified by the evident changes in morphological features and fluorescence labeling (Fig. 2k, left). The elemental mapping (Fig. 2k, right), X-ray photoelectron spectroscopy (XPS) (Supplementary Fig. 10a), and atomic absorption spectroscopy (AAS) (Supplementary Fig. 10b, c) analyses further confirmed the presence of Mn and its surface association, as well as its capability to release from MnLR. Notably, MnLR exhibited a faster Mn release profile in SIF compared with neutral PBS (Supplementary Fig. 10b, c), indicating a release behavior conducive to CRC targeting while limiting off-target distribution. As a result, compared to the raw *L. reuteri*, MnLR exhibited improved proliferation, reuterin production (Fig. 2l, m), as well as biofilm formation and adhesion to colon cancer cells (Supplementary Fig. 11), which would collectively enhance the antitumor efficacy within colon tumor sites. Furthermore, compared with PBS, both raw *L. reuteri* and MnLR exhibited reduced proliferative viability when exposed to simulated gastric fluid (SGF) and SIF (Fig. 2n, o). Nevertheless, MnLR maintained significantly higher growth activity than raw *L. reuteri* under both conditions (Fig. 2n, o), suggesting the protective role of Mn modification in enhancing resistance to gastrointestinal stresses.

MnLR delivered with glycerol inhibits colon cancer cell growth and promotes dendritic cell maturation in vitro

The tumor-inhibitory effect of MnLR delivered with glycerol (MnLR/Gly) was demonstrated in human colon cancer cell lines with diverse MMR statuses—including microsatellite instability-high (MSI-H; SW48, HCT116, RKO), and microsatellite stable (MSS; SW620, DLD-1), as well as in mouse colon cancer cell lines (MC38 and CT26) (Fig. 3a). This effect was attributed to the MnLR-derived glycerol metabolites, as neither *L. reuteri* nor glycerol alone exhibited cytotoxicity to colon cancer cells (Fig. 3a). Moreover, the inhibitory rates of MnLR/Gly were higher than *L. reuteri*/Gly (Fig. 3a) across all the cell types, indicating that Mn promotes *L. reuteri* proliferation and production of cytotoxic metabolites, thus enhancing the cancer cell-killing efficiency. Consistent with the effects observed for *L. reuteri*-derived mixed metabolites, MnLR/Gly exhibited preferential cytotoxicity toward colon cancer cells over non-cancerous cells (Fig. 3a and Supplementary Fig. 12), indicating its anticancer efficacy, alongside reduced toxicity to normal proliferating cells. Further, MnLR/Gly also induced the intracellular generation of cytotoxic ROS (Supplementary Fig. 13a), which has been thought to be a potent initiator of immunogenic cell death (ICD)[43]. Indeed, the cancer cells treated with either pure reuterin or MnLR/Gly underwent a series of biochemical events towards ICD, including the exposure of calreticulin (CRT) on the cellular membrane, and the release of high mobility group box 1 (HMGB1) and adenosine triphosphate (ATP) (Supplementary Fig. 13b–d)[44]. Moreover, Annexin V/PI flow cytometry revealed that MnLR/Gly treatment induced substantial cell death in colon cancer cells, with the apoptotic cell population reaching 42.6%, much higher than 2.0% in untreated cells and 19.2% in reuterin-treated cells (Supplementary Fig. 13e). Consistently, Live/Dead staining confirmed a significantly increased number of dead cells in the MnLR/Gly group (Supplementary Fig. 13f). Together, these results validate that the ICD-associated markers reflect bona fide immunogenic cell death rather than transient stress. These biochemical products generated by the cells experiencing ICD would be engulfed by DCs, stimulating DCs' maturation and facilitating tumor antigen presentation to effector T cells, ultimately priming an antitumor immune response[45]. To investigate this immunological process, we subjected DCs derived from murine bone marrows or human peripheral blood mononuclear cells (mBMDCs or hPBMC-DCs) to the

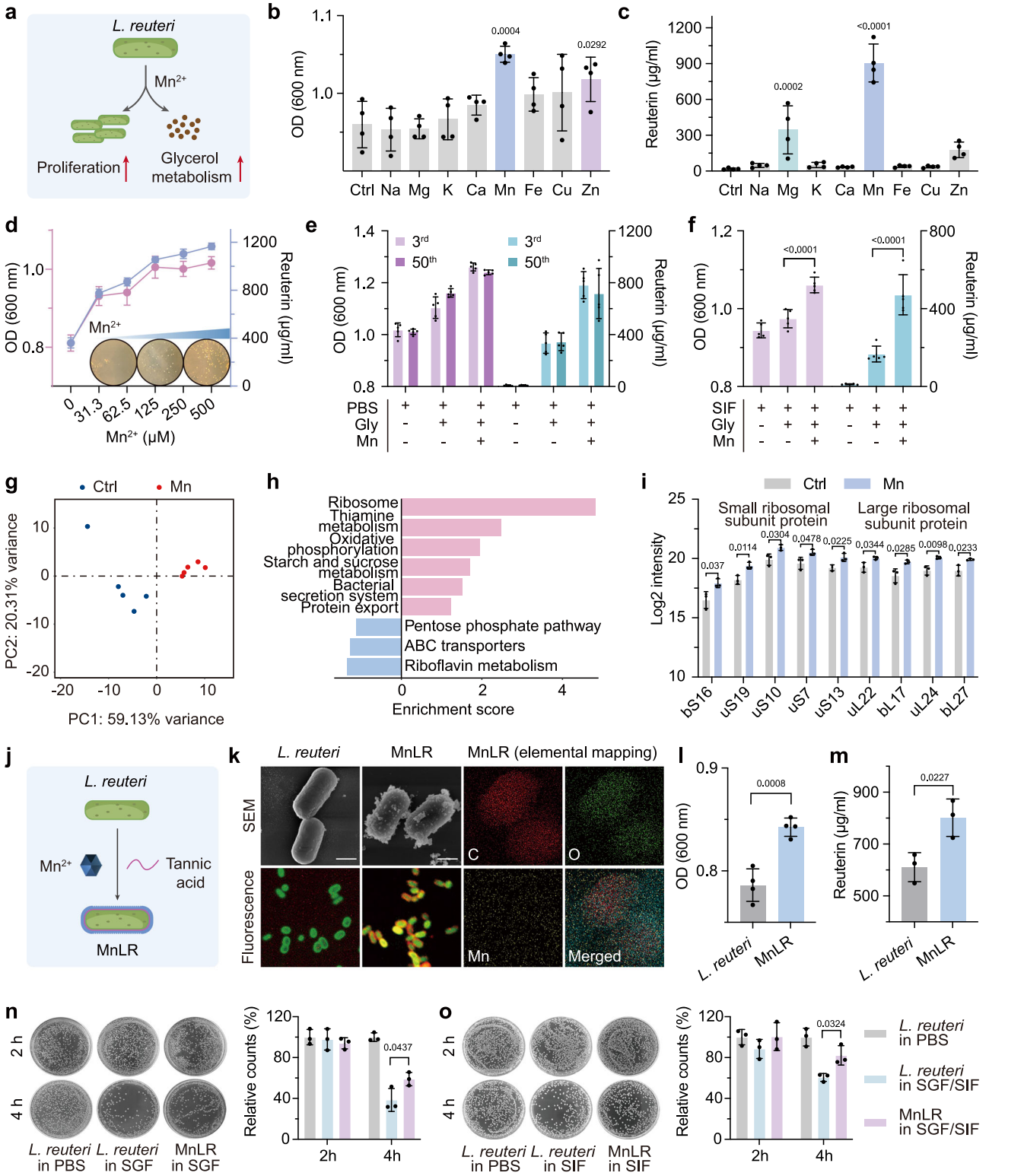

lysates from reuterin- or MnLR/Gly-treated colon cancer cells and observed a significant improvement in DC maturation, as evidenced by the increased proportion of mature DCs ($CD11c^+CD86^+$ mBMDCs and $CD83^+$ hPBMC-DCs), and the production of immune functional cytokines (IL-12, TNF) (Fig. 3b, c and Supplementary Fig. 14). Notably, the lysates from the MnLR/Gly-treated cells exhibited a more pronounced immunostimulatory efficacy on DCs compared with those from the reuterin-treated cells (Fig. 3b, c). These findings collectively indicate the capability of MnLR/Gly to effectively induce ICD in cancer cells to stimulate the functional maturation of DCs, thereby potentially promoting the activation of antitumor immunity (Fig. 3n).

Next, we investigated whether MnLR/Gly had a direct impact on DCs' functional phenotype. Compared with glycerol, TA, and *L. reuteri*, which did not affect the proportion of mature DCs, reuterin, Mn^{2+}, and MnLR all significantly stimulated DCs maturation (Fig. 3d, e and Supplementary Fig. 15). Notably, the proportion of mature DCs was the highest in the MnLR/Gly-treated total DCs (1.7-fold higher than reuterin- or Mn^{2+}-treated mBMDCs, 1.2-fold

Fig. 2 | Screening, preparation, and characterization of MnLR. a The schematic showing the Mn-enhanced proliferation and glycerol metabolism of *L. reuteri*. **b**, **c** The proliferation (measured by the optical density (OD) at 600 nm) and reuterin yield of *L. reuteri* cultured with different metal ions (Na^+, Mg^{2+}, K^+, Ca^{2+}, Mn^{2+}, Fe^{2+}, Cu^{2+}, and Zn^{2+}; 500 μM)) for 18 hours (for proliferation analysis) or 4 hours (for reuterin yield measurement), respectively (n = 4). **d** The proliferation and reuterin yield of *L. reuteri* cultured with Mn^{2+} at different concentrations. The inset, MRS platting assay for analyzing the *L. reuteri* amount after a 24-hour culture with Mn^{2+} (0, 300, and 800 μM) (n = 4). **e** The proliferation and reuterin yield of *L. reuteri* of 3rd or 50th generations cultured with or without Mn^{2+} (n = 5). **f** The proliferation and reuterin yield of *L. reuteri* cultured in SIF with or without Mn^{2+} (n = 5). **g** Principal component analysis (PCA) of gene profiles of untreated and Mn-treated *L. reuteri*. **h** The top nine enriched pathways in Mn-treated *L. reuteri* versus untreated control from Kyoto Encyclopedia of Genes and Genomes (KEGG) enrichment analysis. **i** The quantification of ribosomal proteins of *L. reuteri* with or without Mn^{2+} treatment by LC-MS/MS (n = 3). **j** The schematic presenting the fabrication of MnLR. **k** The representative scanning electronic microscopy (SEM) (Scale bar 1 μm), fluorescence (Scale bar 5 μm), and elemental mapping images of MnLR. CY 3 red fluorescence labels TA; and SYTO 9 green fluorescence labels nucleus. The proliferation and reuterin yield of raw *L. reuteri* and MnLR (**l**, n = 4; **m**, n = 3). **n**, **o** The representative images and corresponding colony counts of raw *L. reuteri* and MnLR cultured in SGF or SIF for 2 or 4 hours (n = 3). The "n" represents the number of biologically independent samples. Data are shown as mean ± SD; p-value (compared to Ctrl in **b**, **c**, **i**); one-way ANOVA (one-tailed), Tukey's multiple comparisons test, or Student's *t*-test for (**e**, **i**, **l**, **m**). Source data are provided as a Source Data file.

higher than reuterin- or Mn^{2+}-treated hPBMC-DCs) (Fig. 3d, e and Supplementary Fig. 15). Inhibition of reuterin production with a GDHt inhibitor reduced DC maturation to the level induced by Mn^{2+} alone (Supplementary Fig. 16), suggesting that glycerol metabolites and Mn^{2+} released by MnLR contribute additively to DC maturation (Fig. 3n). In addition, MnLR/Gly-treated DCs secreted markedly higher levels of IL-12 and TNF than other groups (Fig. 3f, g), further supporting their enhanced functional maturation. To investigate how MnLR/Gly functionally regulates DCs mechanically, we performed RNA-sequencing (RNA-seq) and subsequent pathway enrichment analysis. The results showed that the DEGs in the MnLR/Gly-treated DCs were enriched in the tumor necrosis factor (TNF) signaling pathway and its downstream mitogen-activated protein kinase (MAPK) signaling pathway (Supplementary Fig. 17). Quantitative real-time PCR analysis further confirmed the upregulation of the genes related to these two pathways within MnLR/Gly-treated DCs (Supplementary Fig. 18). The MnLR/Gly-treated DCs also exhibited the increased protein levels of phosphorylated p38 (p-p38) (Fig. 3h, i); and the presence of AMG-548 (a p38 MAPK inhibitor) prevented the MnLR/Gly-induced p38 phosphorylation (Fig. 3h, i) and DCs maturation (Fig. 3j–m). These results suggest that the DCs' maturation driven by MnLR/Gly in part depends on the p38 MAPK pathway.

Altogether, these findings demonstrate that MnLR/Gly can promote dendritic cell maturation, either indirectly by inducing immunogenic tumor cell death through glycerol metabolites or directly by using a combination of glycerol metabolites and Mn ions, thereby potentially enhancing the activation of antitumor immunity (Fig. 3n). This aligns with previous in vivo studies (Fig. 1g–i), indicating that *L. reuteri*-derived glycerol metabolites may regulate DCs in the tumor microenvironment. In addition, the concordance in observations between murine- and human-derived DCs underscores the conserved nature and translational potential of MnLR/Gly-mediated immunomodulation.

MnLR delivered with glycerol drives macrophage polarization towards antitumor phenotype in vitro

Next, we investigated how MnLR/Gly functionally regulated macrophage polarization in vitro, as the previous in vivo experiments (Fig. 1g–i) suggested the potential regulation of macrophage polarization by *L. reuteri*-derived glycerol metabolites. To test M1 (pro-inflammatory and tumor-killing) polarization, we stimulated resting macrophages (RAW264.7 cells, M0) with an M1 inducer (LPS/IFN-γ). MnLR/Gly significantly promoted the M1 polarization, as evidenced by the expanded M1 macrophage subpopulation among total LPS/IFN-γ-stimulated macrophages (Fig. 4a, b), accompanied by the upregulated expression of M1-related markers (Supplementary Fig. 19a), with the M1-promoting efficacy marginally higher than the pure reuterin. By contrast, the macrophage polarization into M2 phenotype (anti-inflammatory and tumor-promoting) was reversed by MnLR/Gly, since the percentage of M2 macrophages (Fig. 4c, d) and the level of M2-related genes (Supplementary Fig. 19b) were drastically decreased in the IL-4 (M2 inducer)-treated RAW264.7 cells with the presence of MnLR/Gly. We also established the 3D multicellular tumor spheroids (MCTs) by co-culturing colon cancer cells and macrophages under LPS/IFN-γ or IL-4 stimulation to investigate the MnLR's antitumor efficacy in the tumor microenvironment containing macrophages. The results showed that the combined presence of MnLR/Gly and LPS/IFN-γ-stimulated macrophages most significantly inhibited MCT growth; meanwhile, MnLR/Gly effectively attenuated IL-4-treated macrophages' stimulatory effects on MCT growth (Fig. 4e and Supplementary Fig. 20), suggesting the synergetic antitumor effects of MnLR/Gly with macrophages in the tumor microenvironment. Of note, glycerol, TA, Mn^{2+}, *L. reuteri*, and MnLR did not affect or even suppress M1 polarization (Supplementary Fig. 21a); while glycerol, Mn^{2+}, and *L. reuteri* also exhibited inhibitory effects on M2 polarization similar to reuterin and MnLR/Gly (Supplementary Fig. 21b). These observations indicate that MnLR-produced glycerol metabolites (especially reuterin) predominately stimulate M1 macrophage polarization, whereas the blockage of M2 macrophage polarization could also be attributed to MnLR-released Mn^{2+} and *L. reuteri* as well as the unmetabolized glycerol, in addition to glycerol metabolites. Human PBMC-macrophages exhibited consistent responses with RAW264.7 cells, wherein MnLR/Gly treatment induced M1 phenotypic polarization (Fig. 4f, g and Supplementary Fig. 22), accompanied by elevated IL-6 and TNF production and enhanced phagocytic activity against colon cancer cells (Fig. 4h–j), thereby reinforcing the robustness and translational potential of immunomodulatory effects mediated by MnLR/Gly.

Furthermore, the subsequent RNA-seq and pathway enrichment analysis revealed that the DEGs in both LPS/IFN-γ- and IL-4-stimulated macrophages with the supplement of MnLR/Gly were markedly enriched in hypoxia-inducible factor 1 (HIF-1) signaling pathway (Supplementary Fig. 23). Quantitative real-time PCR analysis (Supplementary Fig. 24) and immunoblot assay (Fig. 4k, l) further demonstrated the upregulation of HIF-1 signaling pathway-related genes and HIF-1 protein levels within MnLR/Gly-treated macrophages upon LPS/IFN-γ- or IL-4 stimulation. Moreover, the HIF-1 inhibition resulted in reduced M1 macrophages (Fig. 4m, n) but increased M2 macrophages (Fig. 4o, p) under MnLR/Gly treatment, suggesting that the macrophage polarization towards antitumor phenotype induced by MnLR/Gly partially relies on the HIF-1 signaling pathway (Fig. 4t). Consistently, this HIF-1–dependent regulation of macrophage polarization was also validated in human PBMC-macrophages (Fig. 4q–s). Additionally, treatment with the NAC partially reduced MnLR/Gly-induced HIF-1 upregulation, suggesting that this pathway activation is mediated, at least in part, by ROS production (Supplementary Fig. 25).

Together, MnLR/Gly promote the polarization of macrophages towards an antitumor phenotype, thereby enhancing tumor-killing effects.

https://doi.org/10.1038/s41467-025-67437-6

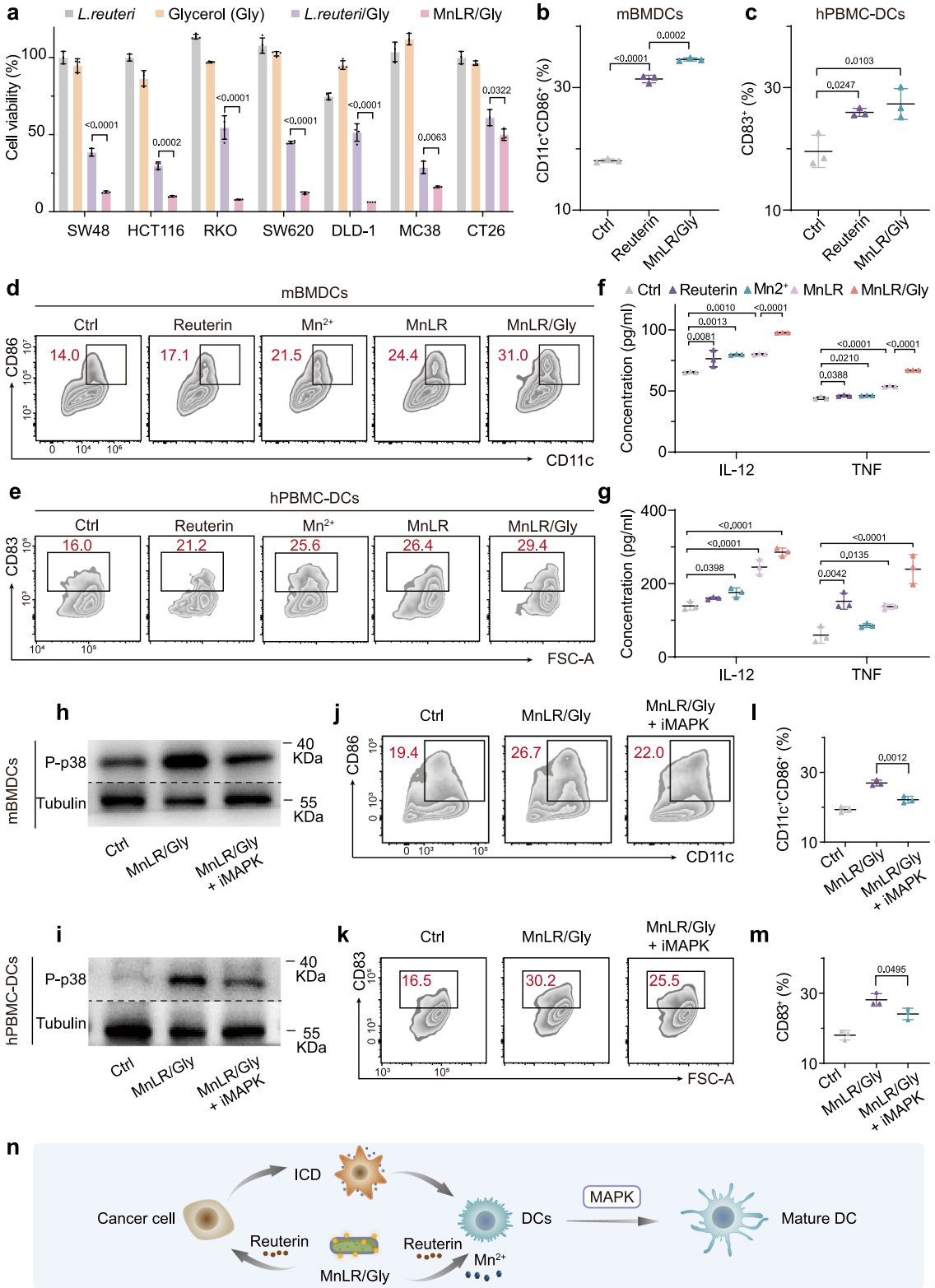

Mn modification improves *L. reuteri* colonization and metabolite distribution at colon tumor sites without eliciting systemic adverse side effects in mice

According to the in vitro observations where MnLR presented an improved proliferative activity, biofilm formation, and adhesion to colon cancer cells, we then determined whether Mn promoted the *L. reuteri* colonization at the colon tumor site in vivo using the orthotopic colon tumor-bearing mice (Fig. 5a). Abundant MnLR arrived at the small intestine and colorectum (tumor site) 1 hour after oral administration, 1.7-fold higher than *L. reuteri* without Mn modification (Fig. 5a, b). The enhanced enrichment of MnLR at the colorectum was maintained for at least 24 hours and was also observed in healthy mice (Fig. 5c–e and Supplementary Fig. 26). Furthermore, *L. reuteri* quantity in the feces from MnLR-treated mice was higher than that from raw *L. reuteri*-treated mice (Fig. 5f), indicating an accelerated proliferation of MnLR in vivo.

Fig. 3 | In vitro colon cancer cell inhibition and DCs maturation mediated by MnLR/Gly. a Cytotoxicity of *L. reuteri*, glycerol, *L. reuteri*/Gly, and MnLR/Gly in multiple human colon cancer cell lines (SW48, HCT116, RKO, SW620, DLD-1) and mouse colon cancer cell lines (MC38, CT26) after a 24-hour incubation (SW48, HCT116, MC38, CT26, n = 3; RKO, SW620, DLD-1, n = 4). **b** Quantification of mature DCs ($CD11c^+CD86^+$) in the total $CD45^+$ mBMDCs after being stimulated by the cell lysates from MC38 cells treated with reuterin or MnLR/Gly (n = 3). **c** Quantification of mature DCs ($CD83^+$) in the total $CD11c^+HLADR^+$ hPBMC-DCs after being stimulated by the cell lysates from DLD-1 cells treated with reuterin or MnLR/Gly (n = 3). **d**, **e** The representative flow cytometric images and corresponding quantification of mature DCs ($CD11c^+CD86^+$ or $CD83^+$) in the total $CD45^+$or $CD11c^+HLADR^+$ DCs after direct stimulation by the given agents (n = 3). **f**, **g** The levels of immune functional cytokines (IL-12, TNF) produced by mBMDCs or hPBMC-DCs after direct stimulation by the given agents (n = 3). **h**, **i** Immunoblotting assays of p-p38 in the mBMDCs or hPBMC-DCs after direct stimulation by the given agents. iMAPK, MAPK inhibitor. Three times were repeated independently with similar results. The representative flow cytometric images (**j**, **k**) and corresponding quantification (**l**, **m**) of mature DCs ($CD11c^+CD86^+$ or $CD83^+$) in the total $CD45^+$ or $CD11c^+HLADR^+$ DCs after the given treatments (n = 3). **n** The schematic showing that MnLR/Gly indirectly (via ICD) or directly promotes DC maturation. Data are shown as mean ± SD; p-value (compared to Ctrl in **f**, **g**); one-way ANOVA (one-tailed), Tukey's multiple comparisons. Source data are provided as a Source Data file.

Of note, both MnLR and raw *L. reuteri* exhibited significantly higher 24-hour retention in the colorectal tissues of tumor-bearing mice compared with healthy mice (Fig. 5d, e and Supplementary Fig. 26). High-resolution ex vivo tissue fluorescence imaging further revealed that MnLR accumulated 1.4-fold more in colon tumor tissues than in adjacent normal tissues (Fig. 5g, h). These observations suggest a preferential localization and colonization of *L. reuteri* in tumor regions, likely influenced by distinct features of the tumor microenvironment (such as oxygen gradients), immunosuppressive states, and tumor-associated alterations of the gut microbiota. Additionally, MnLR preferred to be distributed to the liver, which is the most common metastatic site for CRC[46], rather than other vital organs; and the enrichment of MnLR in the liver was also more significant than that of *L. reuteri* (Supplementary Fig. 27). Next, to determine whether the bioactivity-enhanced MnLR could promote glycerol metabolism and metabolic product accumulation within colon tumor sites in vivo, the orthotopic colon tumor-bearing mice received oral co-gavage with MnLR (or *L. reuteri*) and glycerol for 1 week followed by LC-MS/MS analysis on reuterin content within different tissues (Fig. 5i). Compared to *L. reuteri*/Gly treatment group, higher concentrations of reuterin were found within colon tumors, peripheral blood, and liver of the mice receiving MnLR/Gly treatment (Fig. 5j–l), suggesting an enhanced metabolic activity of MnLR in vivo. Of note, probably due to the poor bioavailability and rapid clearance of reuterin, significantly lower levels of reuterin were detected within colon tumors, peripheral blood, and liver of the mice receiving oral gavage of pure reuterin (Fig. 5j–l). Together, these observations demonstrate the critical role of Mn in facilitating the proliferation, colonization, and antitumor metabolite production of *L. reuteri* at colon tumor sites and in livers in vivo, which would be conducive to improved therapeutic efficacy in primary and even metastatic CRC.

The systemic biosafety of prolonged MnLR/Gly or reuterin treatments was assessed after 30 days of continuous oral administration (100 μl including 10 μl of glycerol and 5×10^9 CFU of *L. reuteri*, once daily) followed by a 3-day withdrawal. Serum biochemical analyses (indicators for key organ functions, lipid profiles, and electrolytes) and histopathological examinations of major organs (heart, liver, spleen, lung, kidney, and intestine) showed no significant abnormalities compared with healthy controls (Supplementary Fig. 28a–f). Likewise, the levels of acute inflammatory cytokines in serum (IL-1β and TNF) returned to baseline after withdrawal, demonstrating the absence of persistent inflammatory responses (Supplementary Fig. 28g). Furthermore, manganese biodistribution analysis revealed that residual Mn levels in serum and major organs after one month of MnLR/Gly administration remained consistent with the physiological manganese concentrations in normal mice (Supplementary Fig. 28h), indicating efficient clearance and the absence of Mn accumulation. These findings demonstrate that MnLR/Gly and reuterin do not induce systemic toxicity and sustained inflammation, highlighting their potential value for clinical translation.

Given the enhanced proliferative and metabolic activity as well as the favorable biosafety of MnLR/Gly observed in vivo, we next investigated its therapeutic and preventive efficacy against CRC in orthotopic and metastatic models.

Oral delivery of MnLR with glycerol effectively inhibits orthotopic colon tumor growth and promotes antitumor macrophages, mature DCs, and effector T cells in mice

Next, we investigated the impacts of oral MnLR/Gly on primary tumor growth using the orthotopically transplanted colon tumor-bearing mice (Fig. 6a). Oral MnLR/Gly significantly suppressed the tumor growth by 95.6%, much higher than reuterin (74.6%), *L. reuteri* (58.4%), and *L. reuteri*/Gly (85%) (Fig. 6b, c and Supplementary Fig. 29). Additional dihydroethidium (DHE) and terminal deoxynucleotidyl transferase dUTP nick end labeling (TUNEL) staining revealed that MnLR/Gly or reuterin administration induced ROS generation and apoptosis in colon tumor tissues, whereas these signals were substantially attenuated in healthy colon tissues (Supplementary Fig. 30). These results further demonstrate in vivo that *L. reuteri*–derived metabolites exert ROS-mediated cytotoxicity selectively on colon tumor tissues, thereby contributing to the minimization of off-target damage to normal tissues consistent with the systemic biosafety confirmation (Supplementary Fig. 30).

To further evaluate the therapeutic potential of MnLR/Gly relative to established colon cancer therapies, we compared its efficacy with 5-fluorouracil (5-FU, a first-line chemotherapy drug), PD-1 antibody (a representative immune checkpoint inhibitor), and panitumumab (an EGFR monoclonal antibody) in the orthotopic colon tumor model. MnLR/Gly achieved a tumor growth inhibition rate 1.14-fold higher than PD-1 antibody, 1.25-fold higher than 5-FU, and 2.9-fold higher than panitumumab (Supplementary Fig. 31). Moreover, MnLR/Gly significantly extended overall survival, with 80% of mice surviving at least 60 days, in contrast to lower survival rates in the other groups (Fig. 6d). These advantages arise from MnLR/Gly's potent antitumor activity, combined with its minimal systemic toxicity, and safe, convenient oral administration. In addition, MnLR/Gly holds promise for lower production costs compared to antibody- or chemotherapy-based regimens, highlighting its potential translational value.

Since MnLR/Gly has demonstrated functional regulation on macrophages and DCs in vitro, we hypothesized that it might similarly impact these tumor-associated immune cells and their downstream elements (such as effector T cells and their antitumor cytokines) in vivo, which could be a critical factor contributing to its enhanced antitumor efficacy. As expected, the activated M1 macrophages ($F4/80^+CD86^+$) and mature DCs ($CD11c^+CD86^+$) were significantly enriched in the tumor tissues of the mice treated with MnLR/Gly, concomitantly with an obvious reduction in M2 macrophages ($F4/80^+CD206^+$) (Fig. 6e, f). Furthermore, MnLR/Gly dramatically promoted the effector T cells activation and antitumor function, as evidenced by the substantially increased enrichment of IFN-γ-expressing $CD4^+$ and $CD8^+$ T cells within the tumor tissues of MnLR/Gly-treated mice, surpassing that observed in *L. reuteri*/Gly-treated mice (Fig. 6e, f). These

https://doi.org/10.1038/s41467-025-67437-6

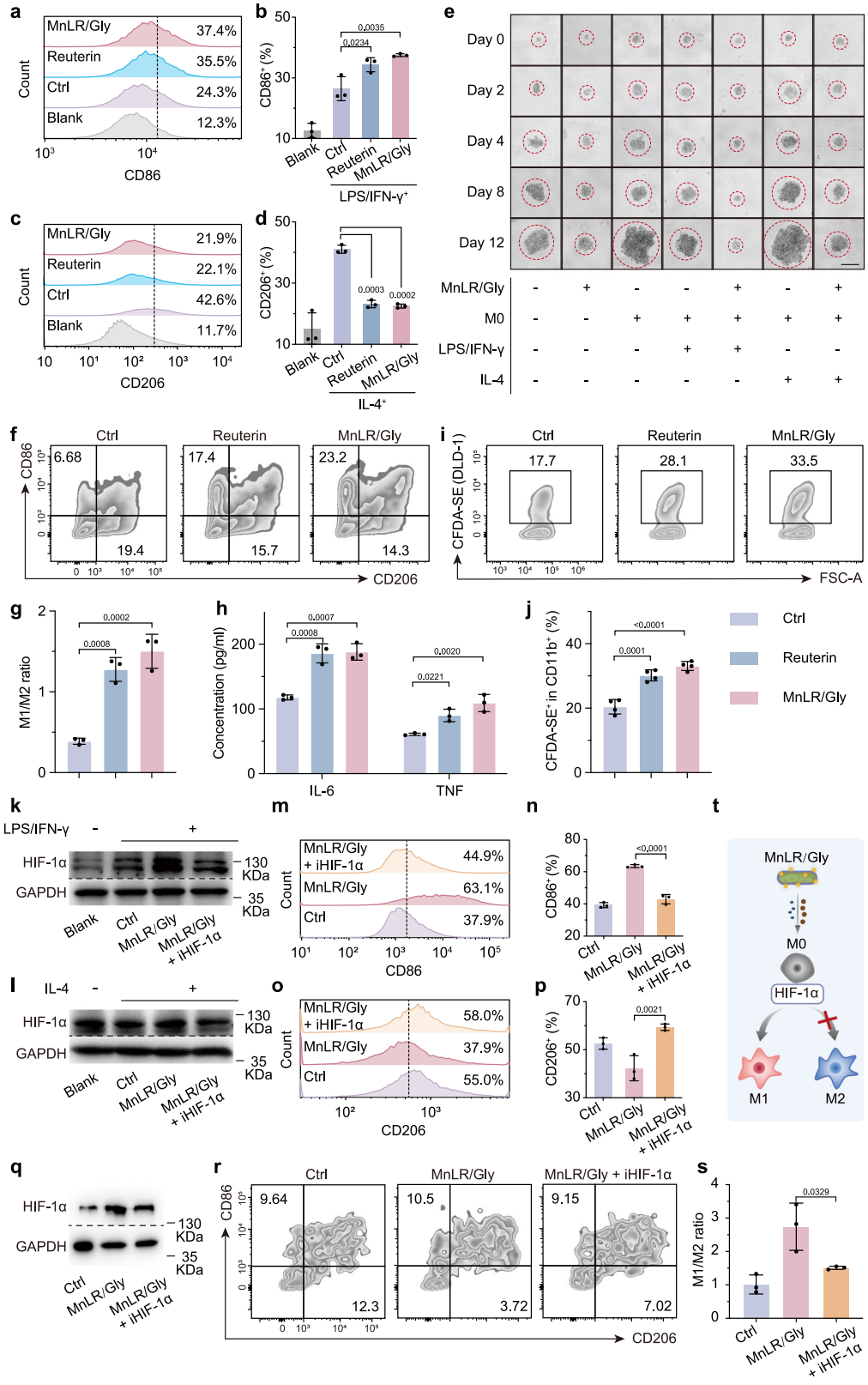

observations suggest that MnLR/Gly actively remodels the tumor immune microenvironment into antitumor in vivo, thus potentiating inhibitory effects on primary colon tumors. We also analyzed the changes of immune cells in the peripheral immune organs, including the spleen and mesenteric lymph nodes (MLNs), which are critical for priming effector T cells and driving systemic antitumor immunity[47,48]. Only the spleens from the mice treated with MnLR/Gly exhibited a simultaneous increase in the ratio of M1 over M2 macrophages, mature DCs, and IFN-γ-expressing $CD4^+$ and $CD8^+$ T cells (Fig. 6g–j and Supplementary Fig. 32). Meanwhile, MnLR/Gly increased the presence of IFN-γ-expressing $CD4^+$ and $CD8^+$ T cells in MLNs (Fig. 6k, l and Supplementary Fig. 33). These data demonstrate the capability of oral MnLR/Gly to stimulate antitumor immune responses beyond local tumor microenvironment, which would be beneficial for preventing

Fig. 4 | MnLR/Gly promotes the polarization of M1 macrophages, meanwhile inhibiting M2 polarization. a, **b** The representative image and corresponding quantification of flow cytometry analysis of M1 ($CD86^+$) polarization in total murine macrophages (RAW264.7 cells) without any treatments (Blank), with only LPS/IFN-γ stimulation (Ctrl), with LPS/IFN-γ stimulation coupled by pure reuterin (Reuterin) or MnL/Gly treatments (n = 3). **c**, **d** The representative image and corresponding quantification of flow cytometry analysis of M2 ($CD206^+$) polarization in total macrophages (RAW264.7 cells) without any treatments (Blank), with only IL-4 stimulation (Ctrl), with IL-4 stimulation coupled by reuterin or MnLR/Gly treatments (n = 3). **e** Images of the 3D MCTs with different treatments at the given time points. The area within the red circle showing the tumor spheroids' morphology. Scale bar, 25 μm. **f**, **g** The representative image and corresponding quantification of flow cytometry analysis of the ratio of M1 ($CD86^+$) to M2 ($CD206^+$) macrophages in $CD45^+CD68^+$ hPBMC-macrophages after reuterin or MnLR/Gly treatments (n = 3). **h** The levels of immune functional cytokines (IL-6, TNF) produced by hPBMC-macrophages after the given treatments (n = 3). **i**, **j** The representative images and corresponding quantification of flow cytometry of the proportion of CFDA-SE^+ cells (DLD-1) in $CD11b^+$ hPBMC-macrophages after being stimulated by the given agents (phagocytic function assessment) (n = 4). **k**, **l** Immunoblotting assays of HIF-1α protein within the RAW264.7 cells with the given treatments. Three times were repeated independently with similar results. The representative image and corresponding quantification of flow cytometry analysis of M1 (**m**, **n**) or M2 (**o**, **p**) polarization in the total LPS/IFN-γ-stimulated or IL-4-stimulated RAW264.7 cells with the given treatments (n = 3). **q** Immunoblotting assays of HIF-1α protein within the hPBMC-macrophages with the given treatments. Three times were repeated independently with similar results. **r**, **s** The representative image and corresponding quantification of flow cytometry analysis of the ratio of M1 ($CD86^+$) to M2 ($CD206^+$) macrophages in $CD45^+CD68^+$ hPBMC-macrophages with the given treatments (n = 3). iHIF-1α, HIF-1α inhibitor (YC-1). **t** The schematic illustration of the impact of MnLR/Gly on macrophage polarization. The "n" represents the number of biologically independent samples. Data are shown as mean ± SD; p-value (compared to Ctrl in **g**, **h**, **j**); one-way ANOVA (one-tailed), Tukey's multiple comparisons. Source data are provided as a Source Data file.

tumor occurrence and metastasis (see the following investigations)[47,49]. Of note, reuterin and *L. reuteri* elicited no significant effects on macrophages, DCs, and effector T cells within the tumor tissues (Fig. 6e, f), suggesting that their suppression of primary colon tumor growth is independent of the antitumor immunity mediated by these three immune cells. Additionally, depleting either $CD8^+$ T cells or macrophages (T dep. or Mac dep.) just attenuated the tumor-inhibitory rate of MnLR/Gly to a level comparable to reuterin, rather than completely offsetting the antitumor effects (Fig. 6b, c and Supplementary Fig. 34). These observations collectively indicate a significant role of the direct cytotoxicity triggered by MnLR-produced metabolites (containing reuterin) in inhibiting primary tumors in vivo. Also, the antitumor immune responses elicited by MnLR/Gly are not confined to a single immune cell type and might even involve the participation of immune cells beyond T cells or macrophages. This might be particularly advantageous for treating tumor subtypes with deficiencies in specific immune cell populations.

We also analyzed the gut microbiota, an important factor influencing tumor growth and the immune microenvironment. Compared with stool samples from healthy mice, those from tumor-bearing mice displayed distinct microbial communities and reduced α-diversity (Fig. 6m and Supplementary Fig. 35a). MnLR/Gly treatment partially ameliorated the colon tumor-induced gut microbiota dysbiosis, concurrently enriching the bacterial genera with potential antitumor properties (including *Lachnoclostridium*[50], *Bacteroides*[51], and *Lactobacillus*[52,53]) (Supplementary Fig. 35b). Moreover, in orthotopic colon tumor-bearing mice pretreated with a cocktail of four broad-spectrum antibiotics to deplete gut microbiota, the inhibitory efficacy of MnLR/Gly on tumor growth was slightly attenuated though not completely abolished (Fig. 6n and Supplementary Fig. 36). These findings indicate that the antitumor effects of MnLR/Gly are mediated in part through gut microbiota modulation, in addition to its immunostimulatory and cytotoxic activities.

Oral delivery of MnLR with glycerol effectively prevents orthotopic primary colon tumor occurrence and liver metastasis in mice

Inspired by the aforementioned capability of MnLR/Gly to initiate systemic antitumor immunity, we subsequently investigated its potential effectiveness in preventing the occurrence of primary colon cancer and mitigating distant metastasis, which is crucial for substantially reducing cancer mortality rates. The mice were administered the given agents via oral gavage once daily for 10 consecutive days, followed by orthotopic inoculation of colon cancer cells and without further treatments (Fig. 7a). The pre-treatment with MnLR/Gly suppressed the formation of a primary colon tumor, resulting in the absence of visible tumor masses in the isolated colon tissues from MnLR/Gly-treated mice on day 14 post tumor inoculation, whereas tumors were developed in colons of the mice in the other treatment groups (Fig. 7b and Supplementary Fig. 37). When the observation period was extended, 75% (6/8) of MnLR/Gly-pretreated mice remained tumor-free for at least 8 weeks (Supplementary Fig. 38a). To further evaluate the durability of the preventive effect of MnLR/Gly, tumor rechallenge experiments were performed by re-inoculating colon cancer cells on day 56 after the initial inoculation in the mice that remained tumor-free following prophylactic treatment of MnLR/Gly (Fig. 7a). Strikingly, 62.5% (5/8) of MnLR/Gly-pretreated mice still exhibited no detectable tumors 3 weeks later (Fig. 7c and Supplementary Fig. 38b), indicating that MnLR/Gly confers a long-lasting protective effect against tumor recurrence. Additionally, the preventive efficacy of MnLR/Gly was validated in a genetic model of spontaneous intestinal tumorigenesis ($Apc^{min/+}$ mice) (Fig. 7d), where continuous oral administration of MnLR/Gly significantly reduced the intestinal tumor multiplicity and the Ki-67–positive proliferating epithelial cells compared with controls (Fig. 7e–h). Collectively, these findings indicate that MnLR/Gly provides durable protection against colorectal tumor development and recurrence, supporting its potential as a preventive strategy for CRC.

Next, we investigated whether the lasting antitumor effects of MnLR/Gly involved the enhanced systemic antitumor immunity. Indeed, MnLR/Gly promoted the splenic macrophage polarization towards M1 phenotype and DC maturation and concomitantly enriched the IFN-γ-expressing $CD4^+$ and $CD8^+$ T cells in MLNs (Fig. 7i–l and Supplementary Fig. 39). ELISA assays further revealed that MnLR/Gly treatment significantly elevated the levels of immune effector cytokines (IFN-γ, TNF, perforin, and granzyme) in serum and MLNs (Supplementary Fig. 40). Consistently, the depletion of $CD8^+$ T cells or macrophages reduced the efficiency of MnLR/Gly in suppressing the formation of primary colon tumors (Fig. 7b and Supplementary Fig. 37). These findings collectively suggest that MnLR/Gly can simultaneously and functionally regulate multiple immune cells across the peripheral immune system in healthy individuals to generate a lasting antitumor effect for preventing colon tumor development.

Next, we determined the potential of MnLR/Gly for preventing colon tumor metastasis by developing a liver metastatic model via splenic injection of colon cancer cells (Fig. 7m). Compared to reuterin and *L. reuteri*/Gly that only reduced tumor burden in spleens, MnLR/Gly demonstrated high efficacy in preventing tumor metastasis into livers, as evidenced by a significant decrease in metastasized liver weight (decrease rate of 35.4%), numbers of metastatic nodules (decrease rate of 62.1%), and tumor invasion area (Fig. 7n–p and Supplementary Fig. 41). Depleting $CD8^+$ T cells or macrophages resulted in reduced efficacy of MnLR/Gly in suppressing formation of liver

https://doi.org/10.1038/s41467-025-67437-6

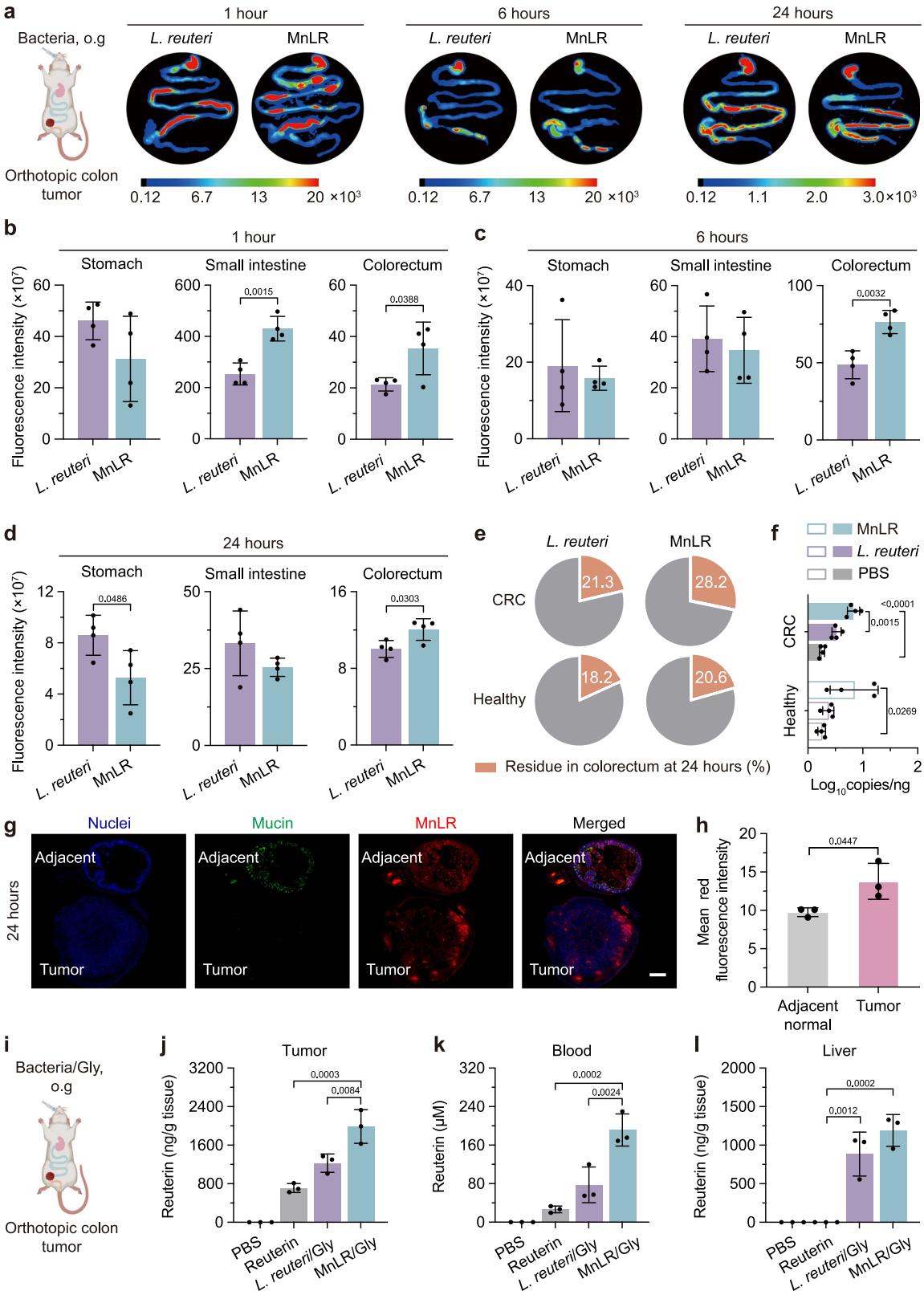

metastatic nodules, highlighting the significance of antitumor immunity for preventing tumor metastasis (Fig. 7n–p).

Together, these results indicate that oral MnLR/Gly can not only suppress primary colon tumor growth but also prevent primary colon tumor development and liver metastases by eliciting effective antitumor immunity, thus revealing MnLR's clinical translation potential in preventing and treating CRC.

GlyMnLR capsule effectively inhibits primary colon tumor growth without eliciting systemic adverse side effects in rabbits

Since the viability of both raw *L. reuteri* and MnLR was lower in SGF than in SIF (Fig. 2n, o), and SEM imaging further revealed that Mn modification was less stable in SGF compared to SIF (Supplementary Fig. 42), we prepared a dimension-tunable enteric-soluble capsule for delivering MnLR encapsulated by glycerol (as one of the capsule

Fig. 5 | Dynamic distribution of oral MnLR and *L. reuteri* within the GI tract. **a** Schematic illustration and the representative fluorescence images of the *L. reuteri* distribution within the GI tract of orthotopic colon tumor-bearing mice 1, 6, and 24 hours after receiving oral gavage with CY 5.5-labeled *L. reuteri* or MnLR. In the schematic illustration, the stomach, small intestine, and colorectum are highlighted in pink, blue, and yellow, respectively; the tumor located at the cecal site is shown in dark red. Created in BioRender. Cao, P. (2025) https://BioRender.com/l8qpogu. **b**–**d** The corresponding statistical analysis of fluorescence signals in the stomach, small intestine, and colorectum at the given time points after oral gavage (n = 4). **e** Proportions of fluorescence signals within the colorectum of healthy and colon tumor-bearing mice 24 hours after oral gavage with *L. reuteri* or MnLR. **f** The quantities of *L. reuteri* in the feces from healthy or colon tumor-bearing mice 24 hours after oral gavage with *L. reuteri* or MnLR (n = 4). **g**, **h** The representative fluorescence images and corresponding quantification of the MnLR distribution in tumor or adjacent normal intestinal tissues (n = 3). Scale bar, 500 μm. **i** Schematic illustration of orthotopic colon tumor-bearing mice receiving the co-gavage of bacteria and glycerol. Created in BioRender. Cao, P. (2025) https://BioRender.com/l8qpogu. Reuterin accumulation in **j** tumor, **k** peripheral blood, and **l** liver of orthotopic colon tumor-bearing mice after receiving the oral gavage of the given agents once daily for 1 week (n = 3). The "n" represents the number of biologically independent samples. Data are shown as mean ± SD; p-value; Student's *t*-test for (**b**–**d**, **h**) or one-way ANOVA (one-tailed), Tukey's multiple comparisons. Source data are provided as a Source Data file.

materials) through 3D printing and casting technology to preserve MnLR bioactivity before reaching the therapeutic targets (Fig. 8a and Supplementary Fig. 43). In vitro and in vivo fluorescence imaging showed that the dissolution rate of the GlyMnLR capsule (MnLR labeled by Cy5.5) was significantly faster in simulated intestinal fluid (SIF) and real intestinal tract compared to simulated gastric fluid and real stomach (SGF) (Fig. 8b, d). This finding was corroborated by endoscopy examination (Supplementary Fig. 44) and X-ray imaging (Fig. 8c), which revealed that the capsule remained intact in the rabbit's stomach for at least 4 hours after oral administration. After reaching the intestine, the barium signal of the capsule was weakened within 20 hours owing to the dissolution of the capsule in intestinal fluid (Fig. 8c). Consistently, in vivo quantitative analysis showed that only ~26.7% of MnLR was released within 4 hours in the stomach, whereas release markedly accelerated during gastrointestinal transit (4–10 hours) and intestinal residence (10–20 hours), with cumulative release reaching ~83.5% within 20 hours (Fig. 8d, e). These observations collectively demonstrated the capsule's resistance to gastric juice and its solubility in the intestinal environment, ensuring sustained and targeted release of MnLR at the site of tumor growth. Next, the orthotopic colorectal tumor model was established in rabbits to investigate the GlyMnLR capsule's antitumor efficacy (Fig. 8f). To optimize the dosing strategy of GlyMnLR capsules, we evaluated three regimens in the model: one capsule every other day, one capsule once daily, and two capsules once daily. Both once-daily regimens achieved stronger tumor suppression than one capsule every other day (approximately 3-fold higher), while the efficacy difference between one and two capsules daily was minimal (Supplementary Fig. 45), with the latter posing greater metabolic burden and safety concerns. The tumor-suppressive efficacy of once-daily oral administration of one GlyMnLR was further confirmed by in vivo CT imaging and photographs of the isolated tumors at the end of the experiments (Fig. 8g–i). Accordingly, we selected one capsule once daily as the optimal dosing regimen for subsequent therapeutic studies. GlyMnLR capsules exhibited a markedly higher tumor inhibition rate (67.9%) compared with free MnLR (25.4%) and reuterin capsules (8.0%), demonstrating the protective role of the enteric formulation and the advantage of sustained production of active metabolites by viable bacteria (Fig. 8j, k). Also, the antitumor efficacy of GlyMnLR capsules was slightly superior to that of the clinically used chemotherapeutic agent 5-FU (Fig. 8j, k), which is consistent with the previous findings in mouse colon tumor models. Immunofluorescence for Ki67 further confirmed the superior inhibitory effect of the GlyMnLR capsule on tumor cell proliferation (Fig. 8l). In addition, GlyMnLR capsules promoted the enrichment of $CD8^+$ T cells in the tumor microenvironment (Fig. 8m, n), supporting the induction of antitumor immunity in the rabbit CRC model. Together with the favorable biosafety profile demonstrated in the rabbit model (Supplementary Fig. 46), these results further support the potential of MnLR to achieve robust antitumor activity while maintaining low toxicity.

Discussion

Probiotics, defined as live microorganisms that confer health benefits to the host when consumed in adequate amounts, have shown promise in various medical aspects primarily through the positive effects on gut health and the immune system, but their use in the treatment of CRC and other cancers is extremely complex and still evolving[54,55]. Typically, current clinical trials predominantly position probiotics as alternative adjuvants to enhance chemotherapeutic or immunotherapeutic efficacy while mitigating side effects by improving pharmacokinetics and body immunity, rather than as standard, standalone antitumor pharmaceuticals[10,55,56]. In this study, we highlight the opportunity of the Mn-modified *L. reuteri* to serve as a primary therapeutic agent and even a preventive approach for alleviating the burden of CRC, one of the most prevalent and lethal types of cancer[1,2]. We elucidated the effectiveness of MnLR in restraining CRC by addressing two primary issues: (1) the mechanistic impacts of MnLR on CRC development (fundamental); and (2) strategies to enhance the bioactivity and bioavailability of *L. reuteri* (applied).

L. reuteri belongs to *Lactobacillus spp.*, one of the most widely used probiotics globally[57]. *L. reuteri* and its metabolites have been used for treating IBD and colic in both animal models and humans[24,58]. Reuterin, which is primarily produced through the metabolism of glycerol by *L. reuteri*, has been studied as an antimicrobial agent[59]. A recent study revealed that reuterin inhibited CRC growth by inducing oxidative stress and inhibiting protein translation[27]. In this study, we confirmed that reuterin exerted cytotoxic effects on colon tumor cells through redox modulation. However, our results suggest that other unidentified components in the glycerol metabolites produced by *L. reuteri* may also contribute to CRC inhibition. According to our compositional analysis of glycerol metabolites, reuterin constituted only 2.48%, with its known downstream metabolites (1,3-PD and 3-HP) accounting for 13.45%. Therefore, it is necessary to further explore and identify other metabolites with tumor-inhibitory effects, which would be critical for mechanistic understanding, therapeutic optimization, and potential biomarker development. More importantly, in addition to the direct cytotoxicity to tumor cells, *L. reuteri* (MnLR) with its glycerol metabolites (including reuterin) was revealed to functionally regulate DCs and macrophages towards antitumor property, and promote the enrichment of effector T cells. This multifaceted immune modulation affected both the tumor microenvironment and key peripheral immune organs (spleen and MLNs). Consequently, oral administration of MnLR and glycerol not only significantly inhibited the growth of the primary colon tumor but also effectively prevented its development and liver metastases. Additionally, oral MnLR with glycerol improved gut dysbiosis induced by colon tumors, which may also be advantageous to the activation of antitumor immunity and improved tumor-inhibitory effects. Collectively, MnLR exerts antitumor effects through multiple biological pathways and holds promise as an independent strategy for CRC treatment and prevention. Nevertheless, the precise molecular and cellular mechanisms underlying these processes warrant further in-depth investigation.

https://doi.org/10.1038/s41467-025-67437-6

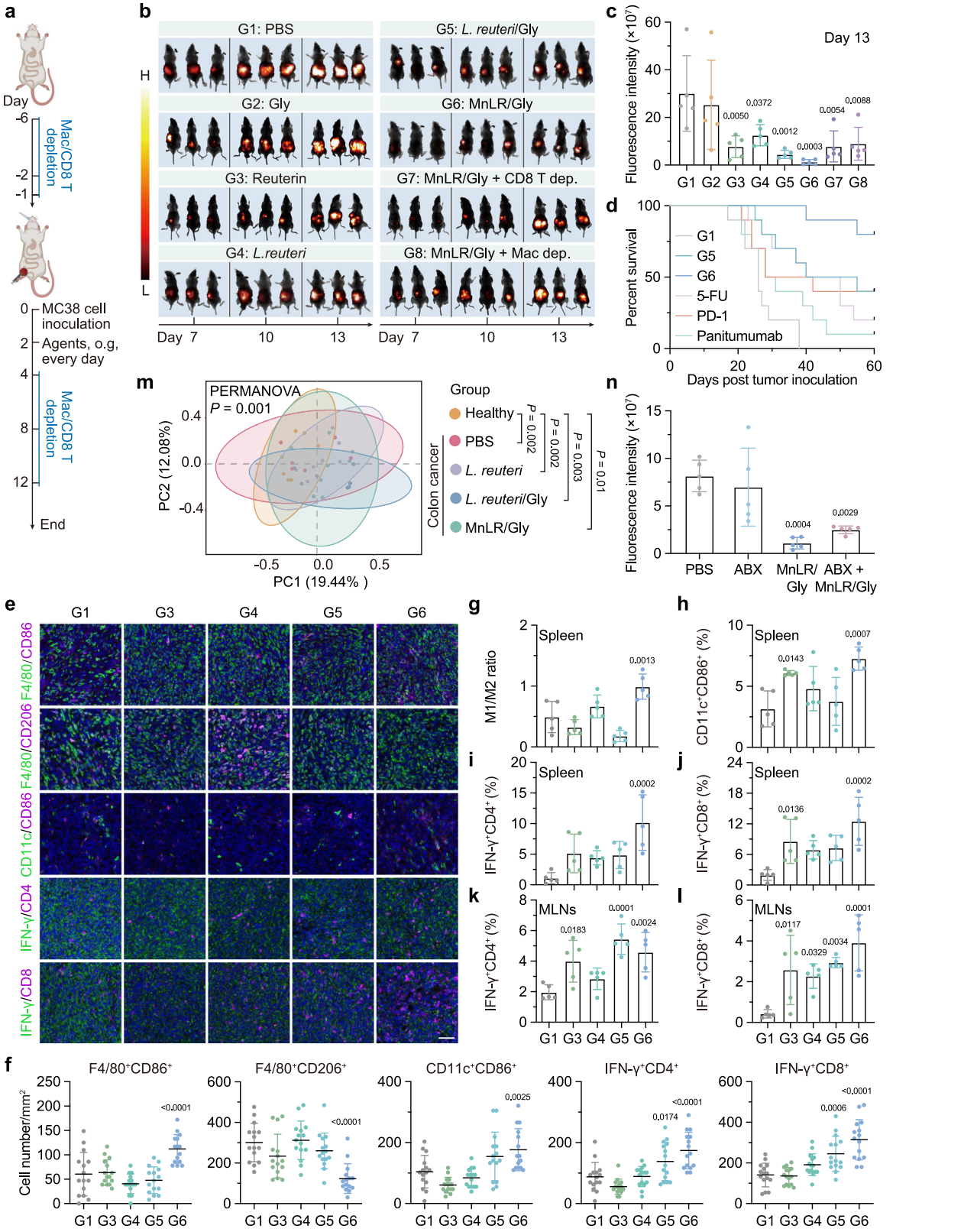

The limited antitumor efficacy poses a significant challenge to the clinical application of probiotics in oncotherapy, since natural probiotics are not specifically in targeting tumors, resulting in insufficient concentrations, activity, and metabolite production of probiotics at the target site to effectively inhibit tumor growth. Although synthetic biology techniques allow for customized gene editing of probiotics to promote the production of specific antitumor substances directly at tumor sites[60–62], their widespread application faces significant challenges, including regulatory hurdles, ethical and public acceptance issues, potential health risks, and the necessity for sophisticated and costly technology to ensure reliability, stability, and repeatability[63]. Additionally, the general applicability of gene editing across various bacterial species remains uncertain. Chemical modification might offer a more straightforward, versatile, and economical approach to

Fig. 6 | In vivo orthotopic colon tumor growth inhibition, gut microbiota modulation, and antitumor immunity activation by oral MnLR/Gly. **a** Schematic illustration of the establishment of primary colon tumor model by orthotopic inoculation of MC38 cells into colon cavity of mice, once-daily oral gavage of the given agents, macrophage or $CD8^+$ T cell (Mac/CD8 T) depletion by clodronate liposomes or anti-CD8 antibody, and analyses on the biological samples (stool, tumor, spleen, and MLNs) isolated from the mice at the endpoint. Created in BioRender. Cao, P. (2025) https://BioRender.com/l8qpogu. **b**, **c** Bioluminescence imaging and the corresponding quantification of the colon tumors in the mice receiving different treatments at the given time points after orthotopic tumor inoculation (n = 5). **d** Survival percentages of colon tumor-bearing mice receiving different treatments (n = 10). **e**, **f** Representative immunofluorescence staining images and the corresponding quantification of M1 macrophages ($F4/80^+CD86^+$), M2 macrophages ($F4/80^+CD206^+$), mature DCs ($CD11c^+CD86^+$), activated $CD4^+$ and $CD8^+$ T cells ($IFN\text{-}\gamma^+CD4^+$ and $IFN\text{-}\gamma^+CD8^+$) within the tumor tissues from the mice receiving the given treatments 14 days after tumor inoculation (n = 15 fields from 3 mice per group). Scale bar, 50 μm. **g**–**j** Quantification of the ratio of M1 to M2 macrophages, and the percentages of mature DCs in total $CD45^+$ cells, activated $CD4^+$ and $CD8^+$ T cells in total $CD3^+$ cells within the spleen from the colon tumor-bearing mice receiving the given treatments 14 days after tumor inoculation (n = 5). **k**, **l** Quantification of the percentages of activated $CD4^+$ and $CD8^+$ T cells in total $CD3^+$ cells within the MLNs from the colon tumor-bearing mice receiving the given treatments 14 days after tumor inoculation (n = 5). **m** Principal component analysis illustrating the β-diversity from 16S rRNA sequencing of stool samples collected from the healthy or primary colon tumor-bearing mice receiving the given treatments on day 14 after tumor inoculation (n = 6 to 8). **n** Quantification of colon tumors in mice at the experimental endpoint under the indicated treatments. Mice were pretreated with antibiotics (ABX) for two weeks prior to tumor cell inoculation to deplete gut microbiota (n = 5). The "n" represents the number of biologically independent samples. Data are shown as mean ± SD; p-value (compared to PBS group); one-way ANOVA (one-tailed), Tukey's multiple comparisons. Source data are provided as a Source Data file.

manipulating bacterial activity and function, as the abundance of surface molecules (polysaccharides, proteins, lipids, and polar functional groups) in bacteria permits various chemical modifications[64]. Metal ions play crucial biological roles in living cells, including bacteria, and can be utilized for customizing live cells through surface modification to enhance their bioactivity and functionality[51,65]. Through screening, we found that Mn ions could promote the proliferation, glycerol metabolism, and colorectal adhesion of *L. reuteri*, and were implicated in regulating the ribosome pathway. Consequently, MnLR with their metabolites were more enriched at the colon tumor sites, peripheral blood, and liver compared to unmodified *L. reuteri*. Nonetheless, we could not exclude the potential protective effect of Mn surface modification on *L. reuteri*, which might also contribute to these observed advantages. Additionally, it remains to be determined whether the bioactivity enhancement by Mn modification is merely specific to *L. reuteri*. Further investigations are needed to confirm if this approach could serve as a universal strategy for improving the targeted therapy of probiotics against CRC. It is also worth noting that Mn^{2+} was reported to directly promote antitumor immune responses by activating cGAS-STING[36,66]. Our results demonstrated that both Mn^{2+} and MnLR promoted DCs maturation, but the effect was significantly weaker compared to MnLR/Gly stimulation, highlighting the critical dual regulatory role of Mn^{2+} and metabolites in DCs maturation. Additionally, transcriptome sequencing revealed that the STING signaling pathway was not significantly upregulated in MnLR/Gly-treated DCs. Consequently, the specific contribution of Mn^{2+} to the immune response and the underlying mechanisms remain unclear. Nevertheless, this Mn modification ultimately benefits the activation of antitumor immunity, through either the direct immunoregulatory effects of Mn^{2+} or its enhancement in the bioactivity of *L. reuteri*.

Withstanding the intense acidity and abundant digestive enzymes in the stomach to successfully colonize the intestines to locally produce sufficient antitumor agents poses a significant challenge for probiotics. To address this, we introduced the enteric capsules to shield MnLR from gastric harshness. Specifically, glycerol was employed as the foundational capsule material to enhance capsules' lubrication, stability, and acid resistance[67,68]. Moreover, once this enteric capsule dissolved in the intestinal tract, it enabled the simultaneous release of MnLR and glycerol within the intestine, thereby facilitating the local production and accumulation of antitumor metabolites at target sites. The robust antitumor efficacy and systemic biosafety of GlyMnLR capsules were demonstrated in the orthotopic colon tumor-bearing rabbit model. To advance the translation of GlyMnLR capsules, further thorough risk assessments and long-term monitoring of biosafety and antitumor efficacy in particularly larger animal models (such as dogs, swine, or potentially nonhuman primates) are needed.

Methods

Human subjects

All procedures involving human participants were approved by the Ethics Committee of Wuhan Union Hospital, Tongji Medical College, Huazhong University of Science and Technology (IORG No. IORG0003571, 2020-S197). Written informed consent was obtained from all participants prior to their inclusion in the study.

Bacterial and cellular culture

L. reuteri strain (ATCC 23272, GDMCC) was cultured in a sealed centrifuge tube containing de Man, Rogosa, and Sharpe (MRS) broth (HB0384, Hopebio, China) or in a carbon dioxide-generating bag containing MRS agar medium to maintain a microaerophilic environment at 37 °C.

Murine colon cancer cells MC38 (CL-0972, Procell, China) and MC38-Luc (YC-A002-Luc-P, Ubigene, China), human colon cancer cells HCT116 (CL-0096), SW48 (CL-0513), RKO (CL-0196), SW620 (CL-0225), DLD-1 (CL-0074) and HT-29 (CL-0118) (Procell, China), human immortalized colonic epithelial cells (NCM460, H1-3701, OriCell, China), human umbilical vein endothelial cells (HUVEC, CP-H082, Procell), human liver cells (L-02, H1-2501, OriCell), and rabbit squamous carcinoma cells (VX2, BFN60700420, BLUEFBIO) were cultured in Dulbecco's Modified Eagle's Medium (DMEM) (C11995500BT, Gibco, USA) containing 10% (v/v) fetal bovine serum (FBS) (10099-141, Gibco, USA). Murine colon cancer cells (CT26, CL-0071, Procell) and macrophage-like cells (RAW264.7, CL-0190, Procell) were cultured in Rosewell Park Memorial Institute (RPMI) 1640 medium (A1049101, Gibco, USA) containing 10% (v/v) FBS. DCs generated from C57BL/6 mouse bone marrows according to our previous work[44] were cultured in RPMI 1640 media containing 10% (v/v) FBS with the supplement of GM-CSF (20 ng/ml) (300-03, PeproTech, USA) and IL-4 (10 ng/ml) (200-04, PeproTech, USA). Peripheral blood mononuclear cells (PBMC), isolated from healthy donors according to the Human PBMC Isolation Kit (071A100.11, IPHASE, China), were cultured in RPMI 1640 media containing 10% (v/v) FBS. All cells were placed in a humidified incubator with 5% CO_2 at 37 °C.

Analysis of *L. reuteri* proliferation, glycerol metabolism, and biofilm formation

L. reuteri was cultured in glycerol solution (500 mM in PBS) containing the given supplements under the microaerophilic environment at 37 °C. After a 4-hour incubation, *L. reuteri* was collected by centrifugation (4000 g, 5 minutes) and resuspended in PBS. The concentration of reuterin in the supernatant was detected by a tryptophan colorimetric method according to previous studies[69]. The GDHt activity of *L. reuteri* was determined using 3-methyl-2-benzothiazoline hydrazone (H693567, Aladdin, China)[70]. For bacterial proliferation assessment, *L. reuteri* was centrifugally collected and resuspended by

https://doi.org/10.1038/s41467-025-67437-6

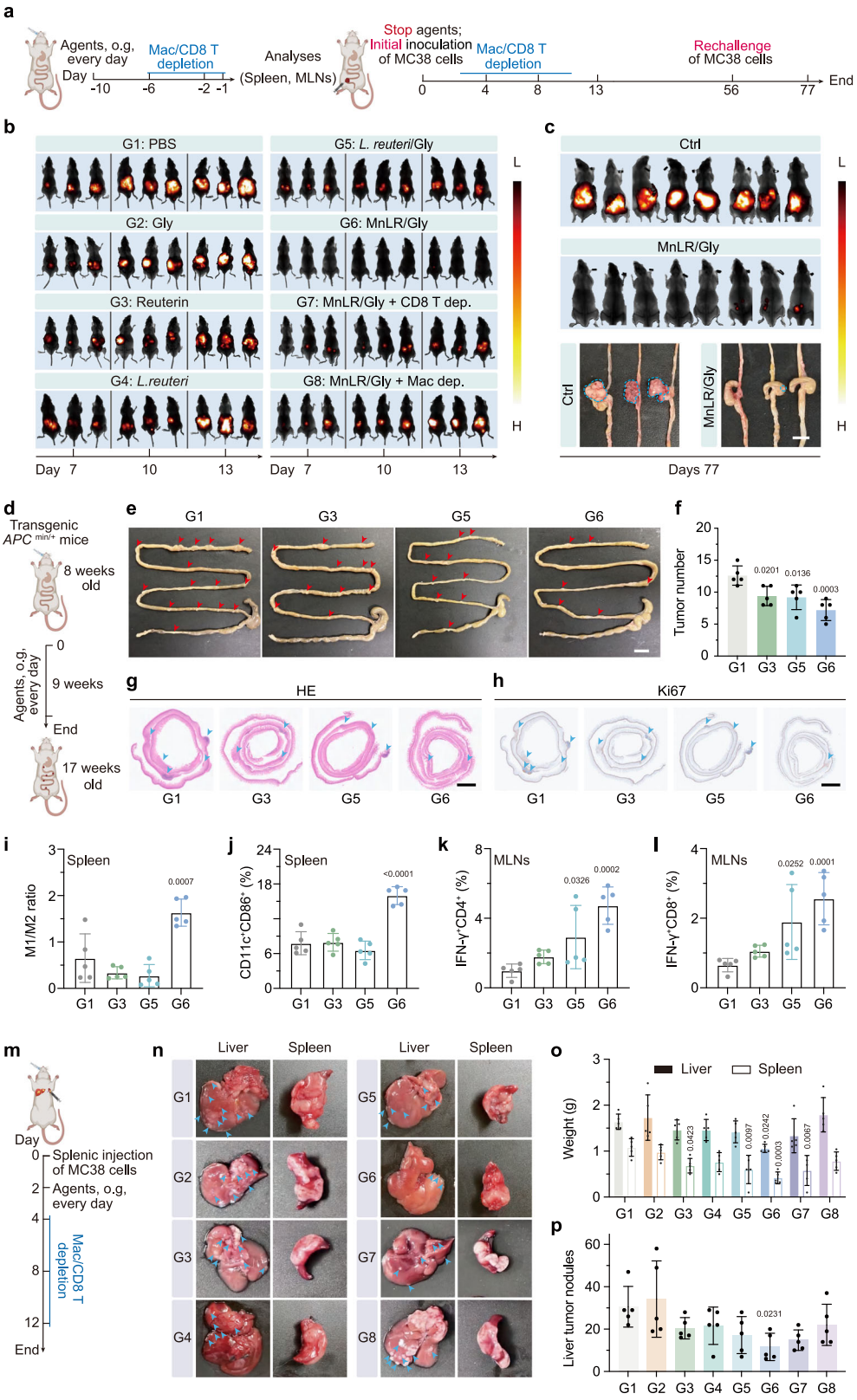

PBS after 18-hour incubation, following absorbance measurement at 600 nm by a multimode reader (RF-5301PC, Japan).

To investigate the bacterial biofilm formation and bio-adhesion, *L. reuteri* in MRS broth (OD600 = 0.8, 500 µl) was seeded in 48-well plates and incubated at 37 °C for 24 hours. The broth was then removed followed by adding 0.5% (w/v) crystal violet (50 µl) to visualize the biofilm production. For bio-adhesion capability assessment, HT-29 cells were seeded in 6-well plates (5×10^5 in 1 ml culture media per well) and cultured for 24 hours. The cells were then washed with HANK's buffer after the removal of culture media. Fresh culture media (2 ml) containing *L. reuteri* or MnLR (10^7 CFU/ml) was added to each well and incubated for 2 hours. After the removal of unattached *L. reuteri* or MnLR in culture media, the cells with attached *L. reuteri* or MnLR were washed with HANK's buffer, digested with trypsin,

Fig. 7 | In vivo prevention of primary colon tumor occurrence and metastasis. **a** Schematic illustration of the pre-treatments with the given agents (once-daily oral gavage for 10 days), biochemical and immunological analyses on blood, spleen, and MLN samples, initial inoculation and rechallenge of colon cancer cells, and macrophage or $CD8^+$ T cell (Mac/CD8 T) depletion. Created in BioRender. Cao, P. (2025) https://BioRender.com/l8qpogu. **b** Bioluminescence imaging of the colon tumors in the mice receiving different treatments at the given time points after initial orthotopic tumor inoculation (n = 5). **c** Bioluminescence imaging and representative images of orthotopic tumor development in mice after the rechallenge of colon cancer cells. The dotted circles mark the location of the tumor. Scale bar, 1 cm. **d** Schematic illustration of the prevention in transgenic $APC^{min/+}$ mice receiving the given treatments for 9 weeks. Created in BioRender. Cao, P. (2025) https://BioRender.com/l8qpogu. **e**, **f** Representative images and the corresponding quantification of tumors in the intestine of $APC^{min/+}$ mice after different treatments (n = 5). Red triangular arrows indicate the tumor nodules. Scale bar, 1 cm. Representative images of H&E staining (**g**) and immunohistochemistry staining of Ki67 (**h**) of the intestinal segments. Blue triangular arrows indicate the tumor nodules. Scale bar, 2.5 mm. **i**, **j** Quantification of the ratio of M1 ($CD11b^+F4/80^+CD86^+$) to M2 ($CD11b^+F4/80^+CD206^+$) macrophages, and the percentages of mature DCs ($CD11c^+CD86^+$) in total $CD45^+$ cells within the spleen from the mice receiving the given treatments for 10 days (n = 5). **k**, **l** Quantification of the percentages of activated $CD4^+$ and $CD8^+$ T cells (IFN-γ^+CD4^+ and IFN-γ^+CD8^+) in total $CD3^+$ cells within the MLNs from the mice receiving the given treatments once daily for 10 days (n = 5). **m** Schematic illustration of the establishment of the liver metastasis model by injecting MC38 cells into the spleen of mice, once-daily oral gavage of the given agents, and macrophage or $CD8^+$ T cell (Mac/CD8 T) depletion. Created in BioRender. Cao, P. (2025) https://BioRender.com/l8qpogu. **n** Representative images of the liver and spleen tissues isolated from the mice 14 days after tumor inoculation. Blue triangular arrows indicate the liver tumor nodules. **o** The weight of livers and spleens isolated from the mice in each group 14 days after tumor implantation (n = 5). **p** The quantification of liver tumor nodules in mice in each group 14 days after tumor inoculation (n = 5). The "n" represents the number of biologically independent samples. Data are shown as mean ± SD; p-value (compared to PBS group); one-way ANOVA (one-tailed), Tukey's multiple comparisons. Source data are provided as a Source Data file.

suspended in PBS, and spread on MRS plates at 10^5 dilutions. *L. reuteri* colonies were counted on the next day. The adhesion rate was calculated as the percentage of *L. reuteri* attached to the cells in the initial total *L. reuteri* number.

Fabrication and characterization of MnLR

L. reuteri was amplified in MRS broth overnight, washed, and resuspended by PBS at a density of ~10^{10} CFU/ml. $MnCl_2$ (100 µl, 1.25 mg/ml) was added to the bacterial suspension (500 µl) and swirled for 30 seconds. TA (100 µl, 5 mg/ml) and PBS (300 µl) were added to the mixture and vortexed for 30 seconds. After a 30-minute standing at 37 °C, MnLR was obtained by centrifugation (4,000 g, 3 minutes). Morphology and element mapping were observed under a biological TEM (FEI Tecnai G2 F20, USA). The presence of Mn and TA within MnLR was determined by XPS (Thermo Scientific K-Alpha, USA) and fluorescence imaging (Nikon Ti-U, Japan).

Evaluation of the stability and retention of MnLR

L. reuteri, cultured overnight in MRS broth, was resuspended in PBS to a density of OD600 of 1.0 and modified with Mn^{2+} to generate MnLR. MnLR or unmodified *L. reuteri* was incubated in simulated gastric fluid (SGF) or simulated intestinal fluid (SIF) at 37 °C for 2 or 4 hours. The bacterial solution was then diluted 4×10^4 times, and 50 µl was evenly spread on an MRS agar medium. Colonies were counted after anaerobic incubation at 37 °C for 24 hours.

In vitro cytotoxicity assay

To investigate the cytotoxicity of metabolites, NCM460, HUVEC, L-02, HCT116, or MC38 were seeded in 96-well plates (5×10^3 cells in 100 µl culture media per well). After a 24-hour incubation, the media were replaced with fresh media containing the given agents. After a 24-hour treatment, the viabilities of these cells were detected by CCK8 assay according to the manufacturer's instructions. To assess the cytotoxicity of MnLR/Gly, NCM460, HUVEC, L-02, CT26, MC38, HCT116, SW48, RKO, SW620, or DLD-1 cells were seeded in the lower chamber of transwell plates (aperture 0.4 µm) (2×10^5 cells 1 ml culture media per well) and cultured for 24 hours. Subsequently, fresh media (0.5 ml) containing *L. reuteri* (10^9 CFU), glycerol (5 µl), *L. reuteri* (10^9 CFU)/Gly (5 µl), or MnLR (10^9 CFU)/Gly (5 µl) were added to the upper chamber. The viabilities of colon cancer cells in the lower chamber were detected by CCK8 assay after a 24-hour incubation.

Colony-forming assay

HCT116 or MC38 cells were seeded in 12-well plates (500 cells in 1 ml culture media per well) and cultured for 48 hours. The cells were treated with the metabolites at the given concentrations for 24 hours, followed by culture medium renewal every 3 days. Colony-forming assays were performed on day 10 (HCT116) or day 15 (MC38 cells) after cell seeding by fixing with 4% paraformaldehyde for 10 minutes, staining with 0.1% crystal violet for 30 minutes, and imaging with an Olympus U-RFL-T microscope (Japan).

Organoid growth assay

Organoids derived from 5 independent CRC patients were prepared according to our previous work[71]. Organoids were embedded in 50 µl of Matrigel (CLS354263, Corning, USA) and cultured with 500 µl of modified medium (PRS-ICM-3D, PRECEDO, China) in 24-well plates. Reuterin (1.5 µg/ml; H916417, Macklin, China) or mixed glycerol metabolites (containing 1.5 µg/ml reuterin) were then added to the plates and incubated for 3 days. Organoids' morphology and size were recorded daily. At the experimental endpoint, organoids were stained with a Live/Dead Cell Staining Kit (C1070, Beyotime Biotechnology, China) and imaged with an Olympus U-RFL-T microscope (Japan).

ROS generation and ICD induction in colon cancer cells

MC38 cells were seeded in the lower chamber of transwell plates (2×10^5 cells in 1 ml culture media per well) and cultured for 24 hours. Fresh media (0.5 ml) containing pure reuterin (18.25 µg/ml) or MnLR (10^9 CFU)/Gly (5 µl) were added to the upper chamber. After a 12-hour incubation, cells were stained with DCFH-DA (Beyotime Biotechnology, China) and imaged with an Olympus U-RFL-T microscope (Japan) to determine intracellular ROS levels. For visualization and location of CRT, cells were stained with anti-CRT/FITC (bs-5913R-FITC, Bioss, China) for 30 minutes at 4 °C. The cells were subsequently stained with Dil membrane dye (S0033, Beyotime Biotechnology, China) for 15 minutes and Hoechst 33342 nuclear dye (14533, Sigma-Aldrich, USA) for another 15 minutes after fixation with 4% paraformaldehyde. Finally, the stained cells were observed under a Nikon Ti-U microscope (Japan) equipped with a CSU-X1 spinning-disk confocal unit (Yokogawa) and an EM-CCD camera (iXon + ; Andor).

DCs maturation

To investigate the DCs maturation stimulated by colon cancer cells undergoing ICD, MC38 or DLD-1 cells were treated with pure reuterin or MnLR/Gly as mentioned above. Subsequently, the cells together with the supernatants in each well were collected and repeatedly frozen-thawed for rapidly lysing cells. The obtained MC38 or DLD-1 cell lysates were then added to the 12-well plates, where murine bone marrow-derived DCs (mBMDCs) or human PBMC-DCs (hPBMC-DCs)

https://doi.org/10.1038/s41467-025-67437-6

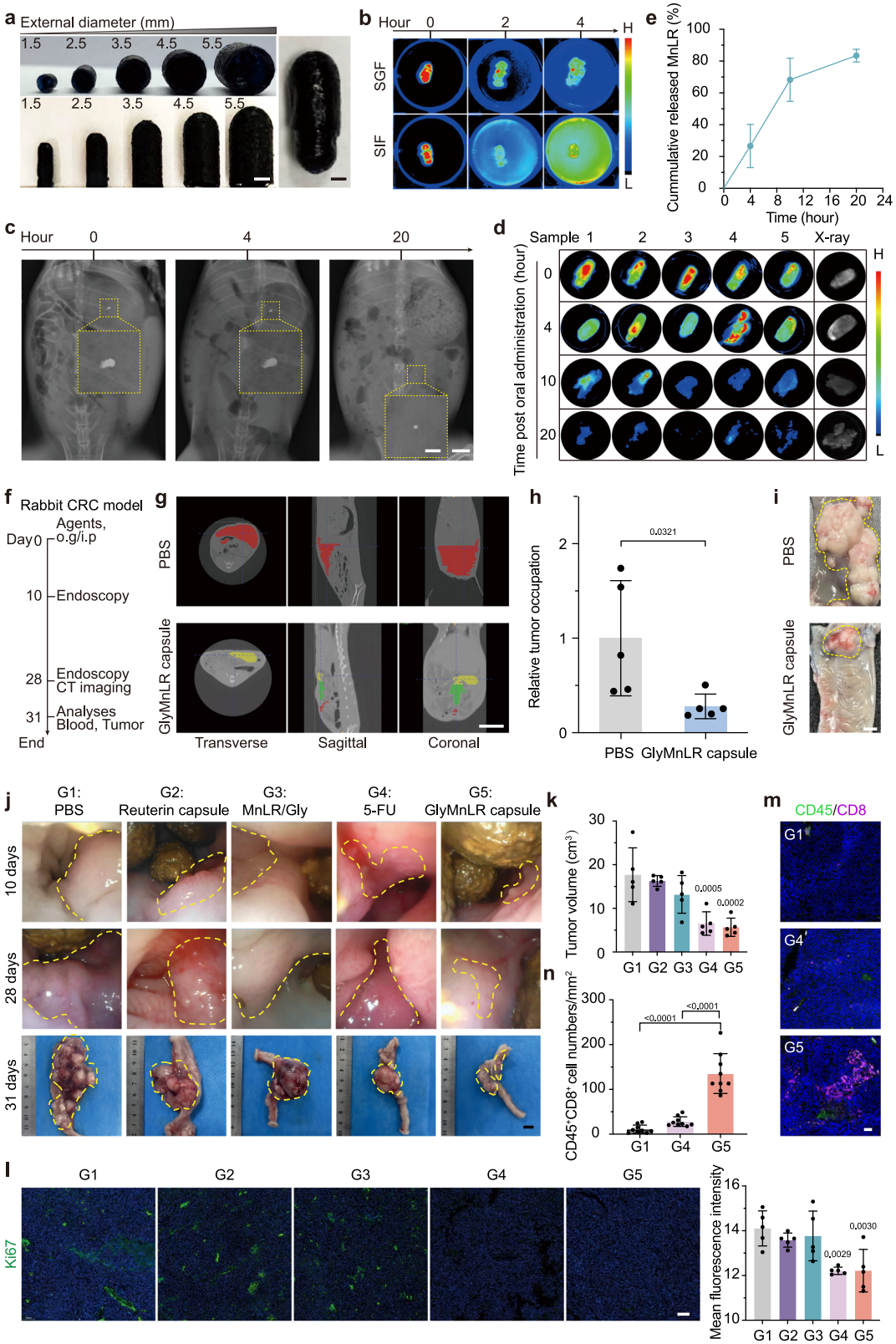

were seeded. After a 24-hour incubation, the DCs in each well were collected for the following analysis. To determine the DCs maturation stimulated by pure reuterin or MnLR/Gly, mBMDCs or hPBMC-DCs were seeded in the lower chamber of transwell plates. Reuterin (6.25 μg/ml) or MnLR (10^9 CFU)/Gly (1 μl) was then added to the upper chamber to stimulate DCs for 24 hours following cell collection and analysis. The percentage of mature DCs in the total DCs collected was determined by flow cytometry analysis (Canto II, BD Company, USA) using the specific antibodies, including CD45-APC/CY 7 (30-F11, 103115), CD11c-BV421 (N418, 117329), and CD86-PE (A17199A, 159204) (BioLegend, USA) for mBMDCs, and CD45-APC/CY 7 (2D1, 368516), CD11c-APC (3.9, 301614), HLA-DR-PerCP/CY 5.5 (L243, 307629), and CD83-PE (HB15e, 305308) for hPBMC-DCs. The Gating strategies were shown in Supplementary Fig. 47. Functional cytokines IL-12 (ELK2507,

Fig. 8 | Characterization of GlyMnLR capsule and its antitumor efficacy and biosafety in rabbit models. a The images of the serial glycerol capsules with different external diameters. Scale bar, 2 mm. **b** Fluorescence images showing the capsule dissolving with the release of CY 5.5-labeled MnLR in SGF and SIF. **c** X-ray images showing the GlyMnLR capsule containing barium sulfate during gastrointestinal transportation after being orally taken by rabbits. Scale bar, 5 mm (left); 2 cm (right). **d**, **e** Fluorescence images of GlyMnLR capsule dissolution and corresponding quantification of MnLR (labeled with CY5.5) release at the given time points after oral administration (n = 5). **f** Schematic illustration of the therapeutic regime, endoscopic/CT imaging, and biochemical and immunological analyses on blood and tumor tissues in the primary CRC-bearing rabbit model. **g** CT images obtained 28 days after the treatment initiation showing the tumor occupation at different locations highlighted by red, yellow, and green colors (Red marks the dense, active core; yellow indicates the infiltrative margin; and green outlines the outer edematous boundary. The color gradient from green to red reflects increasing tumor activity and severity). Scale bar, 5 cm. **h** Quantification of the tumor occupation relative to the PBS group (n = 5). **i** Representative images showing the tumors (highlighted with yellow dashed box) isolated from the primary colon tumor-bearing rabbits 31 days after the treatment initiation. Scale bar, 5 mm. **j** Representative in vivo (endoscopic, the top and middle panels) and ex vivo (the bottom panel) images of tumors (highlighted with yellow dashed boxes) on days 10, 28, and 31 post oral administration of the indicated agents. Scale bar, 1 cm. **k** The tumor volumes obtained from the corresponding groups at the end of the experiment (n = 5). **l** The representative immunofluorescent images and corresponding statistical analysis of the green Ki67-stained proliferating cells within the isolated tumor tissues from rabbits receiving the given treatments at the experimental end (n = 5 fields). Scale bar, 200 μm. **m**, **n** Representative immunofluorescence staining images and corresponding quantification of $CD45^+CD8^+$ T cells within the tumor tissues isolated from the rabbits with the given treatments (n = 9 fields). Scale bar, 50 μm. The "n" represents the number of biologically independent samples. Data are shown as mean ± SD; p-value (compared to PBS group); Student's *t*-test for (**h**) or one-way ANOVA (one-tailed), Tukey's multiple comparisons. Source data are provided as a Source Data file.

ELK2263) and TNF (ELK1387, ELK1190) were measured using the ELISA Kits (ELK Biotechnology, China).

Macrophage polarization

RAW264.7 cells were seeded in the lower chamber of transwell plates (2×10^5 cells in 1 ml culture media per well). M1 and M2 macrophage polarizations were stimulated by LPS (100 ng/ml)/IFN-γ (20 ng/ml) and IL-4 (20 ng/ml), respectively. The hPBMCs were stimulated by recombinant human M-CSF (20 ng/ml) for 6 days to obtain hPBMC-macrophages. After a 24-hour initial stimulation, reuterin (6.25 μg/ml) or MnLR (10^9 CFU)/Gly (1 μl) was added to the upper chamber to further stimulate the macrophages. After 24 hours, the macrophages in each well were collected for subsequent analyses. The percentages of M1 and M2 macrophages in the total RAW264.7 cells macrophages collected were determined by flow cytometry analysis using CD86-PE (A17199A, 159204) and CD206-PE (C068C2, 141706) antibodies (BioLegend, USA), respectively. The M1 ($CD86^+$) to M2 ($CD206^+$) ratio of hPBMC-macrophages was analyzed by flow cytometry using CD45-APC/CY 7 (2D1, 368516), CD68-BV421 (Y1/82 A, 333827), CD86-PE (BU63, 374206), and CD206-APC (15-2, 321110) antibodies (BioLegend, USA). The Gating strategies were shown in Supplementary Fig. 47. The expression of M1-related markers (IL-1β, IL-6, TNF, and iNOS) and M2-related markers (Arg-1, CD206, and Mgl2) was detected by qRT-PCR according to our previous work[44]. The related primer sequences were summarized in the Supplementary Table 3. Functional cytokines (IL-6 and TNF) were measured using the ELISA Kits (ELK Biotechnology, China).

MCTs growth assay

MC38 cells, either alone or mixed with RAW264.7 cells at a 7:3 ratio, were seeded in ultralow-attachment 96-well plates (Corning, USA) (5×10^3 cells in 100 μl culture media per well) and cultured for 48 hours. The suspended MCTs were then harvested and added to the lower chamber of ultralow-attachment 24-transwell plates (Corning, USA). Cytokines (LPS/IFN-γ or IL-4) were supplemented to the culture media with or without the addition of MnLR/Gly to the upper chamber. The culture media were refreshed every two days. The MCTs were imaged at the given time points under an Olympus U-RFL-T microscope (Japan). Their volumes were calculated using the formula: major axis × $(\text{minor axis})^2/2$.

Phagocytosis assay of tumor cells by macrophages

Human PBMC-derived macrophages were stimulated by MnLR/Gly for 24 hours in the 12-transwell plates. DLD-1 cells were labeled with Carboxyfluorescein diacetate succinimidyl ester (CFDA-SE) using the CFDA-SE Cell Proliferation and Tracking Kit (C0051, Beyotime, China) according to the manufacturer's instructions. Subsequently, stimulated or unstimulated macrophages were harvested and mixed with CFDA-SE–labeled DLD-1 cells at a 1:2 ratio, followed by co-culture in 24-well plates for 6 hours. After incubation, cells were gently resuspended, stained with CD11b-BV421 (LM2, 393114, BioLegend, USA) for 30 minutes, washed with PBS, and analyzed by flow cytometry to assess tumor cell phagocytosis. The Gating strategies were shown in Supplementary Fig. 47d.

RNA-seq and pathway analyses

Total RNAs were isolated from DCs or RAW264.7 cells with the given treatments using a TRIzol Reagent Kit (Invitrogen, USA). The RNA quality was evaluated by RNA integrity number (RIN) which above 6 was qualified. Genes with a $|\log_2(\text{fold change})| > 1$ and an adjusted p value < 0.05 were determined to be DEGs. Pathway (*e.g.*, environmental information processing, cellular processes, metabolism, and organismal systems pathway) enrichment analysis was performed with the Kyoto Encyclopedia of Genes and Genomes biological database. The impact of specific signaling pathways, including MAPK p38 and HIF-1, on DC maturation and macrophage polarization was further investigated through qRT-PCR, Western blot, and flow cytometry analyses. The expression of genes related to MAPK p38 and HIF-1 signaling pathways in DCs and macrophages was detected by qRT-PCR (the related primer sequences were summarized in Supplementary Table 3). The protein levels of p38, p-p38, and HIF-1α were determined by western blotting using SAPK4 (E-3) (1:1000, sc-271292, Santa Cruz Biotechnology, USA), Phospho-p38 MAPK-T180/Y182 pAb (1:2000, AP0526, ABclonal Biotechnology, China), and HIF-1α (28b) (1:1000, sc-13515, Santa Cruz Biotechnology, USA) antibodies, respectively. Scans of blots were supplied in the Source Data files. The percentages of mature DCs (mBMDCs and hPBMC-DCs) and M1/M2 macrophages (RAW264.7 and hPBMC-macrophages) were determined by flow cytometry analysis as mentioned above. AMG548 (4100 nM; 52952ES08, YEASEN, China) and YC-1 (10 μM; HY-14927, MedChemExpress, USA) were applied to inhibit MAPK p38 and HIF-1 signaling pathways, respectively.

Animals

Specific pathogen-free (SPF) male C57BL/6 J mice (stock # 000664) (6-8 weeks old) and conventional male New Zealand white rabbits (NZW) (5-8 weeks old) were obtained from the Laboratory Animal Center at Huazhong University of Science and Technology in Wuhan, China. SPF female transgenic $Apc^{min/+}$ mice (B6/JGpt-$Apc^{em1Cin\ (Min)}$/Gpt) (stock # 002020) (8 weeks old) were bought from Shulaibao (Wuhan) Biotechnology Co., Ltd. The experimental/control animals were bred separately with a 12-hour light/dark cycle, 22 °C temperature, and 50% humidity. All animal experiments, including mice and rabbits, were approved by the ethics committee of Tongji Medical College,

Huazhong University of Science and Technology, Wuhan, China (IACUC Number: 2846; 3706). For the subcutaneous tumor, the tumor volume does not exceed 2000 mm^3. For the primary colon tumor, tumor volumes are not directly measured, as tumors are intra-abdominal. Animals are evaluated regularly, and the humane endpoints are defined by a loss of 20% body weight, signs of distress (facial grimace, hunch), difficult breathing, or lackluster hair.

Analyses of antitumor activity and immune cell enrichment in a subcutaneous colon tumor-bearing mouse model

Male C57BL/6 mice were subcutaneously injected with MC38 cell suspension (10^6 cells in 100 µl PBS per mouse) in the right infra-axillary dermis. When the tumor volume reached approximately 50 mm^3, the mice were randomly divided into five groups and intratumorally or orally gavage with PBS, pure reuterin (100 µg per mouse), or mixed metabolite (containing 100 µg reuterin per mouse) once daily. The tumor volumes (calculated by 1/2 × length × $width^2$) were recorded every 2 days. At the experimental endpoint and the tumor volume of mice did not exceed 2000 mm^3, the mice were euthanized by intraperitoneal injection of an overdose of pentobarbital sodium. Tumors in each mouse were isolated for weighing, photographing, and immunofluorescent staining with CD8-CY 3.5 (1:500, ab209775, ABclonal Biotechnology, China), CD11c-CY 3.5 (1:200, 97585S, Cell Signaling Technology, USA), and F4/80-CY 3.5 (1:200, 70076, Cell Signaling Technology, USA). The immune cells in the tumor microenvironment were observed under a Pannoramic MIDI (3DHISTECH, Hungary).

Distribution of *L. reuteri* and reuterin in primary colon tumor-bearing mouse model

The primary colon tumor-bearing mouse model was established by injecting MC38 or MC38-Luc cells (3×10^6 cells in 100 µl PBS per mouse) into the cecal cavity. CY 5.5 dye was used for visualizing *L. reuteri* in vivo. Specifically, NHS-CY 5.5 (50 µg; Q-0363099, Qiyue Biotechnology, China) was added to the *L. reuteri* suspension (10^{10} CFU/ml in 10 ml PBS) and incubated at 37 °C for 15 minutes. *L. reuteri* was then washed with PBS to remove the free dye. CY 5.5-labeled *L. reuteri* was modified with Mn using the same method described in the "Fabrication and characterization of MnLR" section. One week after tumor inoculation, CY 5.5-labeled *L. reuteri* or MnLR (10^9 CFU in 100 µl PBS) was administered to both tumor-bearing and healthy mice. After 1, 6, or 24 hours, the entire GI tracts and other internal organs were isolated and imaged with an in vivo imaging system (IVIS) (BRUKER In-Vivo FX PRO, USA). Subsequent fluorescence quantitative analysis was conducted with the supporting software Bruker MI SE. To investigate the spatial distribution of bacteria within colon tumor tissues and adjacent intestinal tissues, mice were euthanized 24 hours after oral gavage. The isolated tissues were stained with mouse anti-MUC2-FITC (1:100, sc-7314, Santa Cruz Biotechnology, USA) for visualizing the intestinal mucin layer. Quantification of stool *L. reuteri* was achieved through the utilization of qPCR to identify the *pdu* cluster encoding GDHt[72]. Total bacterial DNA was extracted from the stool samples using a Fast DNA Stool Mini kit (51604, QIAGEN, USA). The qPCR amplification was performed by One Step SYBR PrimeScript PLUS Kit (Takara, Japan) on Applied Biosystem StepOne Plus (USA). The *pdu* primer sequences were forward 5′-CCTGAAGTAAAYCGCATCTT-3′ and reverse 5′-GAAACYATTTCAGTTTACGG-3′. The copy number of crude DNA templates in the gut was determined by the correlation of the copy number of serially diluted plasmid DNA standards with cycle threshold run on the same procedure. Quantitative results were expressed as $\log_{10}$ gene copies in 1 ng stool DNA ($\log_{10}$ copies/ng).

To determine the reuterin production and distribution, primary colon tumor-bearing mice were orally gavage with PBS (100 µl per mouse), pure reuterin (100 µg per mouse), *L. reuteri*/Gly, or MnLR/Gly (5×10^9 CFU and 10 µl glycerol per mouse) once daily. One week later, tumor tissues, blood serum, and livers were collected and examined by LC-MS/MS (UltiMate 3000 UHPLCUHPLC/Q Exactive, Thermo Fisher Scientific, USA) for quantifying reuterin.

The biosafety evaluation in mice

For systemic toxicity and inflammatory response assessments, the normal mice received continuous oral administration of MnLR/Gly (100 µl, including 10 µl of glycerol and 5×10^9 CFU of *L. reuteri*, once daily) or reuterin (100 µg, once daily) for 30 days. After a 3-day withdrawal, orbital blood and major organs (heart, liver, spleen, lung, kidney, and intestine) were isolated. Blood samples were collected for biochemical analysis of liver, heart, and kidney function, electrolytes, and lipids with a fully automatic biochemical analyzer (Catalyst One, IDEXX, China), as well as the detection of inflammatory cytokines by ELISA Kits (ELK Biotechnology, China). The isolated organs were fixed with 4% paraformaldehyde, embedded in paraffin, and sliced for haematoxylin and eosin (HE) staining. Residual Mn levels in organs and blood were measured by ICP-OES (Agilent 5800 ICP-OES, Malaysia).

Antitumor activity, gut microbiota, and antitumor immunity assessments in primary colon tumor-bearing mouse model

The primary colon tumor model was established as described above. On the second day after tumor inoculation, mice were orally gavage with the given agents (dosage per mouse: PBS, 100 µl; Glycerol, 10 µl; reuterin, 100 µg; *L. reuteri*/MnLR, 5×10^9 CFU) once daily. To deplete CD8 T cells or macrophages, the tumor-bearing mice were intraperitoneally injected with anti-CD8 (200 µg per mouse; clone 2.43; A2102, Selleck, China) or clodronate-encapsulated liposomes (200 µl per mouse; LIPOSOMA, Netherlands) on days 6, 2, and 1 before tumor inoculation, and on days 4, 8, and 12 following tumor inoculation. For monitoring tumor growth by bioluminescence imaging, the mice (inoculated with MC38-Luc cells) in each group were intraperitoneally injected with D-Luciferin potassium salt (150 mg/kg mouse weight; Y023738, Beyotime Biotechnology, China) and imaged by IVIS. At the experimental endpoint (day 14 after tumor inoculation) and the weight loss did not exceed 20% according to humane endpoint criteria, the mice were euthanized and intestines were isolated from the mice in each group for observing and photographing tumors. Additionally, stool samples were collected for 16S rRNA sequencing analysis to reveal gut microorganisms (OE Biotech, China). Gut microbiota depletion was induced by administering an antibiotic cocktail (consisting of ampicillin (A433389), neomycin (N109017), and metronidazole (M109874) (0.2 g/L each) together with vancomycin (0.1 g/L, V301569) (Aladdin, China)) in the drinking water for two weeks prior to tumor cell inoculation.

To compare MnLR/Gly with current standard-of-care treatments, the orthotopic colon tumor-bearing mice were treated with MnLR/Gly daily as mentioned above or (1) PD-1 antibody (RMP1-14; A2122, Selleck, China; 100 µg once every three days, i.p.), (2) 5-FU (F476739, Aladdin, China; 400 µg every other day, i.p.), and (3) Panitumumab (A2018, Selleck, China; 200 µg once every three days, i.p.). The tumor growth was recorded weekly, and mouse survival was evaluated using Kaplan-Meier analysis until spontaneous death occurred or the end of the 2-month observation period.

To assess the antitumor immunity, colon tumor tissues, spleens, and MLNs were isolated from the mice in each group on day 14 after tumor inoculation. The tumor tissues were fixed with 4% paraformaldehyde and stained with the specific antibodies, including F4/80-FITC (1:1000, 70076), CD86-CY 5 (19589), CD11c-FITC (1:1000, 97585S), CD206-CY 5 (1:1000, 24595) (Cell Signaling Technology, USA), IFN-γ-FITC (1:400, Df6045, Affinity Biosciences, China), CD4-CY 5 (1:400, Ab183685, Abcam, China), and CD8-CY 5 (1:4000, Ab209775, Abcam, China). Spleens and MLNs were dissociated into single-cell

suspensions, stained with antibodies, and then washed and resuspended with PBS. Collected cell samples were analyzed by flow cytometry. The following antibodies were used: CD45-BV510 (30-F11), CD11c-PE/CY 7 (N418), CD86-APC (GL-1), CD11b-FITC (M1/70), F480-BV421 (BM8), CD206-PE (C068C2), CD3-APC (17A2), CD4-FITC (RM4-5), CD8-Percp/CY 5.5 (53-6.7), and IFN-γ-PE (XMG1.2) (BioLegend, USA). The Gating strategies were shown in Supplementary Fig. 47.

Evaluation of the preventive effects on primary colon tumor occurrence and liver metastasis in mouse model

To evaluate the preventive effects on primary colon tumor occurrence, mice were orally administered the given agents once daily. 10 days later, the mice ceased oral medication and received the injection of MC38-Luc cells (3×10^6 cells in 100 μl PBS per mouse) into their cecal cavity, followed by tumor growth monitoring. On day 14 after tumor inoculation, the intestines were isolated from the mice for observing and photographing tumors. The agent dosage, methods for depleting CD8 T cells or macrophages, tumor growth monitoring approach with IVIS, and the procedures for analyzing immune cells in spleens and MLNs using flow cytometry have been described in detail in the previous section. The levels of perforin (ELK3068), granzyme (ELK1660), TNF, and IFN-γ (ELK1132) in both serum and MLNs were measured by ELISA Kits (ELK Biotechnology, China).

For the tumor rechallenge study, healthy mice were first pretreated with MnLR/Gly by oral gavage for 10 consecutive days, followed by orthotopic inoculation with MC38 cells. MnLR/Gly administration was discontinued thereafter. At week 8 post-initial inoculation, tumor growth was evaluated, and mice that remained tumor-free were subjected to a second orthotopic MC38 cell inoculation. Age-matched mice receiving tumor inoculation at the same time point served as controls. Tumor growth was visualized and quantified by IVIS after 3 weeks. For the *Apc*$^{min/+}$ transgenic mouse model, 8-week-old mice were randomly divided into 4 groups and orally administered with the given agents daily. After 9 weeks of treatment, mice were euthanized, and intestinal tissues were harvested for HE staining and Ki67 (1:200, 9129, Cell Signaling Technology, USA) immunohistochemical analysis.

To investigate the inhibitory effects on liver metastasis of colon cancer, mice received a splenic injection of MC38 cells (5×10^5 cells in 100 μl PBS per mouse). Swabs were employed to massage the spleen for 5 minutes to accelerate cell flow into the hepatic portal vein. On the second day after tumor inoculation, mice were orally gavaged with the given agents. The agent dosage and methods for depleting CD8 T cells or macrophages were the same as mentioned above. On day 14 after tumor inoculation, spleens and livers were harvested from the mice in each group for weighing, photographing, counting of tumor nodules, and histological analysis.

Fabrication of GlyMnLR capsules

The rod-shaped master molds (with a length of 10 mm) for the capsule's outer (4 mm in diameter) and inner (3 mm in diameter) shells were designed with the Solidworks 2021 software and printed in an X190 3D printer (JGAURORA, China) using polylactic acid (PLA) (Jiguang Erwo Technology, China) as the raw materials. The negative molds were fabricated from the master molds using polydimethylsiloxane (PDMS) (PHR1518, Sigma-Aldrich, USA). The precursor solution for capsule shells was prepared by mixing glycerol (2 ml) and gelatin (2 g) in ddH_2O (4 ml). The mixture was placed in an oven at 75 °C for approximately 30 minutes until the gelatin was fully dissolved. Genipin (2% w/v; G101204 Aladdin, China) was added to the mixture that was subsequently filled into the negative PDMS molds. The rod-shaped PLA molds with diameters of 2 mm (for outer shell) or 1 mm (for inner shell) produced by 3D printing were vertically inserted into the mixture and left for 5 minutes to form the capsule cavity. The gel-like capsule shell precursors fully solidified after being placed at 37 °C for 2 days. The negative molds were then removed to obtain the outer capsule shell with a diameter of 3.5 mm and the inner capsule shell with a diameter of 2.5 mm. The outer and inner shells were cut to lengths of 5 mm, and following joined together to form the complete capsule with a length of 8 mm. The enteric-coated polymer was prepared by dissolving 200 mg of Eudragit L-100 (P756765, Macklin, China) in an organic solvent mixture containing 1 ml of dichloromethane (Sinopharm, China) and 1 ml of anhydrous ethanol (Sinopharm, China), followed by stirring until the solution became transparent. The polymer solution was then cast to the capsule's surface for 3 times. The coated capsules were left to dry at 37 °C for 24 hours, resulting in the formation of enteric-coated capsules. MnLR (10^{11} CFU in 20 μl PBS) was slowly injected into the capsule using a syringe to obtain the final MnLR. This specific size of GlyMnLR capsules was used in subsequent in vitro and in vivo experiments. Capsule shells of other sizes presented in Fig. 8b were prepared using the same method.

Monitoring of GlyMnLR capsule dissolution and *L. reuteri* release in the GI tract

To observe the capsule dissolution and *L. reuteri* release in vitro, capsules loaded with CY 5.5-labeled MnLR were immersed into the SGF (pH 2.0, containing 0.01 M HCl and 3.2 g/l pepsin) or SIF (pH 6.8, containing 0.01 M PBS, 0.2 M NaOH, and 10 g/l trypsin) and imaged by IVIS. To further determine GlyMnLR capsules' resistance against gastric fluid in vivo, they were administered to the throats of rabbits that had been fasted for 2 days to assist with active swallowing, followed by endoscopic observation (Endoscope, Yuyanbio, China). Finally, to demonstrate that the capsules can dissolve in intestinal fluids, the rabbits were orally administered capsules containing barium sulfate for abdominal radiographic imaging using an X-ray photographic system (Mindray, China). For Quantitative analysis of capsule dissolution kinetics and MnLR release in vivo, capsules loaded with Cy5.5-labeled MnLR were administered to rabbits by oral gavage. Four experimental groups were euthanized at designated time points: immediately (0 h), 4 h, 10 h, and 20 h post-gavage. Rabbits were euthanized by first inducing deep anesthesia with isoflurane inhalation, followed by an intravenous injection of an overdose of pentobarbital sodium through the auricular vein. In the first group (0 h), the capsule was immediately retrieved from the stomach and imaged to determine the initial fluorescence intensity ($Intensity_0$). In the second group (4 h), the capsule was recovered from the stomach, and the remaining fluorescence ($Intensity_4$) was measured; the cumulative release at 4 h was calculated as $(Intensity_0 - Intensity_4)/Intensity_0 \times 100\%$. In the third and fourth groups, capsules retrieved from the intestinal tract at 10 h and 20 h were similarly imaged, and cumulative release fractions were computed. Fluorescent imaging was performed using IVIS to quantify residual capsule signal in situ.

Antitumor activity and biosafety assessments in the CRC rabbit model

To establish the primary colon cancer model in rabbits, VX2 cell suspension (2×10^8 cells in 200 μl PBS) was inoculated into the thigh muscle of 5-week-old rabbits. After 4 weeks, the resulting solid tumors in the muscles were excised and minced with surgical scissors in a petri dish. The tumor tissues were then transferred to a homogenizer and processed by grinding no more than five times. The homogenized tissues were suspended in sterile PBS, centrifuged at 4 °C (2000 g, 5 minutes), washed twice, resuspended by PBS, and injected into the colon wall (approximately 5 cm below the cecum along the median abdominal line) of 6-8-week-old rabbits (500 μl tumor suspension per rabbit). Two days later, the tumor-bearing rabbits were administered with the given agents for one month: (1) PBS, once daily (o.g.), (2) GlyMnLR, one capsule every other day, one capsule once daily, or two capsules once daily (o.g.), (3) free MnLR/Gly, once daily (o.g.), (4) one

reuterin (2 mg) capsule, once daily (o.g.), and (5) 5-FU, 20 mg/kg every three days (i.p.). Tumor progression was monitored at designated time points by CT imaging (SOMATOM, Siemens, Germany) and endoscopic examination (YAN-E30, YUYAN INSTRUMENTS, China). On day 31 and the weight loss did not exceed 20% according to humane endpoint criteria, the rabbits were euthanized and tumors in each group were finally isolated for ex vivo imaging, Ki67 staining, and immunofluorescence staining with rabbit-specific antibodies against CD45 (1:1000, L12/201, LS-C187600) and CD8 (1:200, 12.C7, LS-C187471) (LSBio, USA).

To assess the systemic toxicity, tumor-free rabbits (6-8 weeks old) received the GlyMnLR capsule once daily for one month. Blood samples were then collected and biochemically analyzed in the same way as in the previous section.

Statistical information

All experiments were performed at least 3 times. Data were presented as mean ± standard deviation (SD). Statistical analyses were conducted using Student's *t*-test for comparisons between two independent groups and one-way ANOVA with Tukey's post-hoc tests for comparisons among three or more independent groups. Statistical significance was indicated by the p-value.

Reporting summary

Further information on research design is available in the Nature Portfolio Reporting Summary linked to this article.

Data availability

The sequencing data have been deposited in NCBI under the PRJNA1245031. All data are included in the Supplementary Information or available from the authors, as are unique reagents used in this Article. The raw numbers for charts and graphs are available in the Source Data file whenever possible. Source data are provided with this paper.

References

1. Sung, H. et al. Global Cancer Statistics 2020: GLOBOCAN estimates of incidence and mortality worldwide for 36 cancers in 185 countries. *CA Cancer J. Clin.* **71**, 209–249 (2021).
2. Siegel, R. L., Miller, K. D., Wagle, N. S. & Jemal, A. Cancer statistics, 2023. *CA Cancer J. Clin.* **73**, 17–48 (2023).
3. Guo, C. G. et al. Aspirin use and risk of colorectal cancer among older adults. *JAMA Oncol.* **7**, 428–435 (2021).
4. Chan, A. T. et al. Long-term use of aspirin and nonsteroidal anti-inflammatory drugs and risk of colorectal cancer. *JAMA* **294**, 914–923 (2005).
5. Thompson, P. A. et al. Celecoxib for the prevention of colorectal adenomas: results of a suspended randomized controlled trial. *J. Natl. Cancer Inst.* **108**, djw151 (2016).
6. Overman, M. J. et al. Nivolumab in patients with metastatic DNA mismatch repair-deficient or microsatellite instability-high colorectal cancer (CheckMate 142): an open-label, multicentre, phase 2 study. *Lancet Oncol.* **18**, 1182–1191 (2017).
7. Christofides, A. et al. The complex role of tumor-infiltrating macrophages. *Nat. Immunol.* **23**, 1148–1156 (2022).
8. Park, E. M. et al. Targeting the gut and tumor microbiota in cancer. *Nat. Med.* **28**, 690–703 (2022).
9. Wong, C. C. & Yu, J. Gut microbiota in colorectal cancer development and therapy. *Nat. Rev. Clin. Oncol.* **20**, 429–452 (2023).
10. Wang, L. et al. Gut microbiome in tumorigenesis and therapy of colorectal cancer. *J. Cell. Physiol.* **238**, 94–108 (2023).
11. Zitvogel, L., Daillère, R., Roberti, M. P., Routy, B. & Kroemer, G. Anticancer effects of the microbiome and its products. *Nat. Rev. Microbiol.* **15**, 465–478 (2017).
12. Qu, R. et al. Role of the gut microbiota and its metabolites in tumorigenesis or development of colorectal cancer. *Adv. Sci.* **10**, e2205563 (2023).
13. Baruch, E. N. et al. Fecal microbiota transplant promotes response in immunotherapy-refractory melanoma patients. *Science* **371**, 602–609 (2021).
14. Fong, W. et al. Lactobacillus gallinarum-derived metabolites boost anti-PD1 efficacy in colorectal cancer by inhibiting regulatory T cells through modulating IDO1/Kyn/AHR axis. *Gut* **72**, 2272–2285 (2023).
15. Chen, Y. E. et al. Engineered skin bacteria induce antitumor T cell responses against melanoma. *Science* **380**, 203–210 (2023).
16. Feng, Q. et al. Engineered bacterial outer membrane vesicles as controllable two-way adaptors to activate macrophage phagocytosis for improved tumor immunotherapy. *Adv. Mater.* **34**, e2206200 (2022).
17. Chen, Y. et al. Reinforcement of the intestinal mucosal barrier via mucus-penetrating PEGylated bacteria. *Nat. Biomed. Eng.* **8**, 823–841 (2024).
18. Pan, J. et al. A single-cell nanocoating of probiotics for enhanced amelioration of antibiotic-associated diarrhea. *Nat. Commun.* **13**, 2117 (2022).
19. Coutzac, C. et al. Systemic short chain fatty acids limit antitumor effect of CTLA-4 blockade in hosts with cancer. *Nat. Commun.* **11**, 2168 (2020).
20. Cao, F. et al. Engineering clinically relevant probiotics with switchable "Nano-Promoter" and "Nano-Effector" for precision tumor therapy. *Adv. Mater.* **36**, e2304257 (2024).
21. Jones, S. E. & Versalovic, J. Probiotic Lactobacillus reuteri biofilms produce antimicrobial and anti-inflammatory factors. *BMC Microbiol.* **9**, 35 (2009).
22. Thomas, C. M. et al. FolC2-mediated folate metabolism contributes to suppression of inflammation by probiotic Lactobacillus reuteri. *MicrobiologyOpen* **5**, 802–818 (2016).
23. Gu, Q., Zhang, C., Song, D., Li, P. & Zhu, X. Enhancing vitamin B12 content in soy-yogurt by Lactobacillus reuteri. *Int. J. Food Microbiol.* **206**, 56–59 (2015).
24. Sung, V. et al. Lactobacillus reuteri to treat infant colic: a meta-analysis. *Pediatrics* **141**, e20171811 (2018).
25. Riezzo, G. et al. Randomised double blind placebo controlled trial on Lactobacillus reuteri DSM 17938: improvement in symptoms and bowel habit in functional constipation. *Benef. Microbes* **9**, 51–60 (2018).
26. Zhao, Y. et al. Two novel lactic acid bacteria, Limosilactobacillus fermentum MN-LF23 and Lactobacillus gasseri MN-LG80, inhibited Helicobacter pylori infection in C57BL/6 mice. *Food Funct.* **13**, 11061–11069 (2022).
27. Bell, H. N. et al. Reuterin in the healthy gut microbiome suppresses colorectal cancer growth through altering redox balance. *Cancer Cell* **40**, 185–200.e186 (2022).
28. Bender, M. J. et al. Dietary tryptophan metabolite released by intratumoral Lactobacillus reuteri facilitates immune checkpoint inhibitor treatment. *Cell* **186**, 1846–1862.e1826 (2023).
29. Frei, A., Verderosa, A. D., Elliott, A. G., Zuegg, J. & Blaskovich, M. A. T. Metals to combat antimicrobial resistance. *Nat. Rev. Chem.* **7**, 202–224 (2023).
30. Palmer, L. D. & Skaar, E. P. Transition metals and virulence in bacteria. *Annu. Rev. Genet.* **50**, 67–91 (2016).
31. Zhang, X. et al. Characterization of metal binding of bifunctional kinase/phosphatase AceK and implication in activity modulation. *Sci. Rep.* **9**, 9198 (2019).
32. Martínez-Rodríguez, S. et al. Metal-triggered changes in the stability and secondary structure of a tetrameric dihydropyrimidinase: a biophysical characterization. *Biophys. Chem.* **139**, 42–52 (2009).

33. Jakubovics, N. S., Smith, A. W. & Jenkinson, H. F. Oxidative stress tolerance is manganese (Mn(2+)) regulated in Streptococcus gordonii. *Microbiology* **148**, 3255–3263 (2002).
34. Culotta, V. C. & Daly, M. J. Manganese complexes: diverse metabolic routes to oxidative stress resistance in prokaryotes and yeast. *Antioxid. Redox Signal.* **19**, 933–944 (2013).
35. Qian, K. et al. Manganese enhances macrophage defense against Mycobacterium tuberculosis via the STING-TNF signaling pathway. *Int. Immunopharmacol.* **113**, 109471 (2022).
36. Lv, M. et al. Manganese is critical for antitumor immune responses via cGAS-STING and improves the efficacy of clinical immunotherapy. *Cell Res.* **30**, 966–979 (2020).
37. Drost, J. & Clevers, H. Organoids in cancer research. *Nat. Rev. Cancer* **18**, 407–418 (2018).
38. Ganesh, K. et al. Immunotherapy in colorectal cancer: rationale, challenges and potential. *Nat. Rev. Gastroenterol. Hepatol.* **16**, 361–375 (2019).
39. Cañellas-Socias, A., Sancho, E. & Batlle, E. Mechanisms of metastatic colorectal cancer. *Nat. Rev. Gastroenterol. Hepatol.* **21**, 609–625 (2024).
40. Wang, Y. et al. Tumor-draining lymph nodes: opportunities, challenges, and future directions in colorectal cancer immunotherapy. *J. Immunother. Cancer* **12**, e008026 (2024).
41. Dishisha, T., Pereyra, L. P., Pyo, S. H., Britton, R. A. & Hatti-Kaul, R. Flux analysis of the Lactobacillus reuteri propanediol-utilization pathway for production of 3-hydroxypropionaldehyde, 3-hydroxypropionic acid and 1,3-propanediol from glycerol. *Microb. Cell Fact.* **13**, 76 (2014).
42. Dai, X. & Zhu, M. Coupling of ribosome synthesis and translational capacity with cell growth. *Trends Biochem. Sci.* **45**, 681–692 (2020).
43. Li, Q. et al. NIR-responsive hollow germanium nanospheres mediate photothermal/photodynamic therapy and restrain immunosuppression to cooperatively eradicate primary and metastatic tumors. *Chem. Eng. J.* **458**, 141314 (2023).
44. Li, Q. et al. IDO-inhibitor potentiated immunogenic chemotherapy abolishes primary tumor growth and eradicates metastatic lesions by targeting distinct compartments within tumor microenvironment. *Biomaterials* **269**, 120388 (2021).
45. Peng, K., Zheng, Y., Xia, W. & Mao, Z. W. Organometallic anti-tumor agents: targeting from biomolecules to dynamic bioprocesses. *Chem. Soc. Rev.* **52**, 2790–2832 (2023).
46. Zhou, H. et al. Colorectal liver metastasis: molecular mechanism and interventional therapy. *Signal Transduct. Target. Ther.* **7**, 70 (2022).
47. Hiam-Galvez, K. J., Allen, B. M. & Spitzer, M. H. Systemic immunity in cancer. *Nat. Rev. Cancer* **21**, 345–359 (2021).
48. Li, Y. et al. Hydrogel dual delivered celecoxib and anti-PD-1 synergistically improve antitumor immunity. *Oncoimmunology* **5**, e1074374 (2016).
49. Patras, L., Shaashua, L., Matei, I. & Lyden, D. Immune determinants of the pre-metastatic niche. *Cancer Cell* **41**, 546–572 (2023).
50. Zhu, G. et al. Intratumour microbiome associated with the infiltration of cytotoxic CD8+ T cells and patient survival in cutaneous melanoma. *Eur. J. Cancer* **151**, 25–34 (2021).
51. Tintelnot, J. et al. Microbiota-derived 3-IAA influences chemotherapy efficacy in pancreatic cancer. *Nature* **615**, 168–174 (2023).
52. Zhang, Q. et al. Lactobacillus plantarum-derived indole-3-lactic acid ameliorates colorectal tumorigenesis via epigenetic regulation of CD8(+) T cell immunity. *Cell Metab.* **35**, 943–960.e949 (2023).
53. Kawanabe-Matsuda, H. et al. Dietary Lactobacillus-derived exopolysaccharide enhances immune-checkpoint blockade therapy. *Cancer Discov.* **12**, 1336–1355 (2022).
54. Redman, M. G., Ward, E. J. & Phillips, R. S. The efficacy and safety of probiotics in people with cancer: a systematic review. *Ann. Oncol.* **25**, 1919–1929 (2014).
55. Ting, N. L., Lau, H. C. & Yu, J. Cancer pharmacomicrobiomics: targeting microbiota to optimise cancer therapy outcomes. *Gut* **71**, 1412–1425 (2022).
56. He, Y. et al. Gut microbial metabolites facilitate anticancer therapy efficacy by modulating cytotoxic CD8(+) T cell immunity. *Cell Metab.* **33**, 988–1000.e1007 (2021).
57. Luo, M. et al. Preventive effect of Lactobacillus reuteri on melanoma. *Biomed. Pharmacother.* **126**, 109929 (2020).
58. Dias, A. M. M. et al. Lactobacillus stress protein GroEL prevents colonic inflammation. *J. Gastroenterol.* **56**, 442–455 (2021).
59. Sun, M. C. et al. Application of the reuterin system as food preservative or health-promoting agent: a critical review. *Foods* **11**, 4000 (2022).
60. Gurbatri, C. R. et al. Engineered probiotics for local tumor delivery of checkpoint blockade nanobodies. *Sci. Transl. Med.* **12**, eaax0876 (2020).
61. Chowdhury, S. et al. Programmable bacteria induce durable tumor regression and systemic antitumor immunity. *Nat. Med.* **25**, 1057–1063 (2019).
62. Canale, F. P. et al. Metabolic modulation of tumours with engineered bacteria for immunotherapy. *Nature* **598**, 662–666 (2021).
63. Kumar, P., Sinha, R. & Shukla, P. Artificial intelligence and synthetic biology approaches for human gut microbiome. *Crit. Rev. Food Sci. Nutr.* **62**, 2103–2121 (2022).
64. Lin, S. et al. Surface-modified bacteria: synthesis, functionalization and biomedical applications. *Chem. Soc. Rev.* **52**, 6617–6643 (2023).
65. Cao, F. et al. Artificial-enzymes-armed Bifidobacterium longum probiotics for alleviating intestinal inflammation and microbiota dysbiosis. *Nat. Nanotechnol.* **18**, 617–627 (2023).
66. Zhao, Z. et al. Mn(2+) directly activates cGAS and structural analysis suggests Mn(2+) induces a noncanonical catalytic synthesis of 2'3'-cGAMP. *Cell Rep.* **32**, 108053 (2020).
67. Zhang, Y., Zhao, Q., Wang, H., Jiang, X. & Cha, R. Preparation of green and gelatin-free nanocrystalline cellulose capsules. *Carbohydr. Polym.* **164**, 358–363 (2017).
68. Yan, C., Cao, H. & Xu, M. Producing and quality control of fecal-derived microbiota enteric capsules. *Chin. J. Digestion* **36**, 407–411 (2016).
69. Spinler, J. K. et al. Human-derived probiotic Lactobacillus reuteri demonstrate antimicrobial activities targeting diverse enteric bacterial pathogens. *Anaerobe* **14**, 166–171 (2008).
70. Toraya, T., Ushio, K., Fukui, S. & Hogenkamp, P. C. Studies on the mechanism of the adenosylcobalamin-dependent diol dehydrase reaction by the use of analogs of the coenzyme. *J. Biol. Chem.* **252**, 963–970 (1977).
71. Wang, X. et al. A tumor-organoid-based precision medicine platform for the prediction of drug sensitivity of colorectal cancer. *Adv. Therap.* **5**, 2200093 (2022).
72. Frese, S. A. et al. The evolution of host specialization in the vertebrate gut symbiont Lactobacillus reuteri. *PLoS Genet.* **7**, e1001314 (2011).

Acknowledgements

This study was supported by the Noncommunicable Chronic Diseases-National Science and Technology Major Project (2023ZD0509904 to Z.W., 2023ZD0509900 to Z.W.), National Key Research and Development Program of China (2022YFC2408100 to L.W.), the National Natural Science Foundation of China (82272277 to L.W., 81974382 to Z.W., 82173315 to Z.W., 82302585 to Q.L.), Major Scientific and Technological Innovation Projects of Hubei Province (2022BCA013 to Z.W.), Hubei Province Science and Technology Innovation Team Project No. 11, the Natural Science Foundation of Hubei Province (2022CFB736 to L.W.), Wuhan Natural Science Foundation Exploration Program (Chenguang Program 2024040801020348 to Q.L.).

Author contributions

Z.W., L.W., W.C., P.C., and Q.L. conceived and designed the study. P.C., Q.L., Y.L., H.G., C.W., R.X., and C.OY. performed the experiments. P.C. and Q.L. participated in data analysis. The manuscript was written and supervised by Z.W., L.W., Q.L., and P.C.

Competing interests

The authors declare no competing interests.

Additional information

Supplementary information The online version contains supplementary material available at https://doi.org/10.1038/s41467-025-67437-6.

Correspondence and requests for materials should be addressed to Wei Chen, Lin Wang or Zheng Wang.

Peer review information *Nature Communications* thanks Jiahe Li who co-reviewed with Marwa El-DeranyMichael Linnebacher and the other anonymous reviewer(s) for their contribution to the peer review of this work. A peer review file is available.

[1]Department of Clinical Laboratory, Union Hospital, Tongji Medical College, Huazhong University of Science and Technology, Wuhan, China. [2]Research Center for Tissue Engineering and Regenerative Medicine, Union Hospital, Tongji Medical College, Huazhong University of Science and Technology, Wuhan, China. [3]Hubei Key Laboratory of Regenerative Medicine and Multi-disciplinary Translational Research, Wuhan, China. [4]Hubei Provincial Engineering Research Center of Clinical Laboratory and Active Health Smart Equipment, Wuhan, China. [5]Department of Pharmacology, School of Basic Medicine, State Key Laboratory for Diagnosis and Treatment of Severe Zoonotic Infectious Diseases, Tongji-Rongcheng Center for Biomedicine, Tongji Medical College, Huazhong University of Science and Technology, Wuhan, China. [6]Hubei Key Laboratory for Drug Target Research and Pharmacodynamic Evaluation, Huazhong University of Science and Technology, Wuhan, China. [7]Key Laboratory of Biological Targeted Therapy (Huazhong University of Science and Technology), Ministry of Education, Wuhan, China. [8]Department of Gastrointestinal Surgery, Union Hospital, Tongji Medical College, Huazhong University of Science and Technology, Wuhan, China. [9]These authors contributed equally: Peng Cao, Qilin Li. ✉e-mail: weichen86@hust.edu.cn; lin_wang@hust.edu.cn; zhengwang@hust.edu.cn